



HAL
open science

The rise and demise of Iran's Urmia Lake during the Holocene and the Anthropocene: "what's past is prologue"

Arash Sharifi, Morteza Djamali, Larry Peterson, Peter Swart, María Guadalupe Pulido Ávila, Mojgan Esfahaninejad, Jacques-Louis de Beaulieu, Hamid Lahijani, Ali Pourmand

► To cite this version:

Arash Sharifi, Morteza Djamali, Larry Peterson, Peter Swart, María Guadalupe Pulido Ávila, et al.. The rise and demise of Iran's Urmia Lake during the Holocene and the Anthropocene: "what's past is prologue". *Regional Environmental Change*, 2023, 23 (4), pp.121. 10.1007/s10113-023-02119-x . hal-04204286

HAL Id: hal-04204286


<https://amu.hal.science/hal-04204286v1>

Submitted on 12 Sep 2023

HAL is a multi-disciplinary open access archive for the deposit and dissemination of scientific research documents, whether they are published or not. The documents may come from teaching and research institutions in France or abroad, or from public or private research centers.

L'archive ouverte pluridisciplinaire **HAL**, est destinée au dépôt et à la diffusion de documents scientifiques de niveau recherche, publiés ou non, émanant des établissements d'enseignement et de recherche français ou étrangers, des laboratoires publics ou privés.

The rise and demise of Iran's Urmia Lake during the Holocene and the Anthropocene: "what's past is prologue"

Arash Sharifi^{1,2,3}  Morteza Djamali⁴ · Larry C. Peterson² · Peter K. Swart² · María Guadalupe Pulido Ávila^{5,6} · Mojgan Esfahaninejad⁷ · Jacques-Louis de Beaulieu⁴ · Hamid A. K. Lahijani⁸ · Ali Pourmand^{1,2}

Received: 19 December 2022 / Accepted: 29 August 2023

Abstract

Urmia Lake in NW Iran was the world's second largest hypersaline lake until three decades ago, when it began to lose ~ 90% of its surface area due to dwindling water input and enhanced evaporation. To help discern the role of natural vs anthropogenic factors in the rapid demise of Urmia Lake, we present a high-resolution, multi-proxy reconstruction of climate, and hydrological variability from the lake's sediments. We identify several episodes of wet and dry conditions over the past 11,300 years, and an atmospheric teleconnection between the climate of the interior of West Asia and the North Atlantic region. Estimates of mean annual precipitation based on chemical weathering indices range between 174 and 401 mm year⁻¹ during the Holocene. A combination of geochemical proxies, pollen reconstruction, and the absence of any evaporite horizons throughout the Holocene period point to the prevailing role of human impact on the current vanishing of Urmia Lake.

Keywords Urmia Lake · Hypersaline Lake · Holocene · Anthropocene · Paleorainfall · Human impact · Iran paleoclimate · Medieval Warm Period · Little Ice Age

Introduction

Urmia Lake (NW Iran, 37°29'49"N, 46°00'34"E, 1275 m.a.s.l.) has long been considered the second largest hypersaline lake in the world and, until three decades ago, the largest land-locked body of water in Iran. The lake and its

unique associated habitats were incorporated in the Ramsar Convention on Wetlands of International Importance in 1975. In the early 1990s, the government of Iran established a water management program within the Urmia Lake watershed, which decreased the flux of water to lower than the average flow measured over 60 years (1955–1995) (Sharifi et al. 2018b). Although evidence is mounting that human

Communicated by Juan Ignacio Lopez Moreno

✉ Arash Sharifi
osharifi@earth.miami.edu

✉ Ali Pourmand
apourmand@earth.miami.edu

¹ Neptune Isotope Laboratory (NIL), Department of Marine Geosciences, Rosenstiel School of Marine, Atmospheric & Earth Science, University of Miami, 4600 Rickenbacker Causeway, Miami, FL 33149-1098, USA

² Department of Marine Geosciences, Department of Marine Geosciences, Rosenstiel School of Marine, Atmospheric & Earth Science, 4600 Rickenbacker Causeway, Miami, FL 33149-1098, USA

³ Beta Analytic-Isobar Science, Research and Development Department, 4985 SW 74th Ct, Miami, FL 33155, USA

⁴ Institut Méditerranéen de biodiversité et d'Ecologie (IMBE – UMR CNRS 7263 / IRD 237 / Aix-Marseille Univ/Avignon

Université), Europôle Méditerranéen de l'Arbois, BP 80, 13545 cedex 04 Aix-en-Provence, France

⁵ Laboratorio de Palinología, Instituto de Botánica, Departamento de Botánica y Zoología, Universidad de Guadalajara, Camino Ramón Padilla 2100, Las Agujas, Nextipac, C.P. 45200 Zapopan, Jalisco, México

⁶ Laboratorio Nacional de Identificación y Caracterización Vegetal (LaniVeg-CONACYT), Departamento de Botánica y Zoología, Universidad de Guadalajara, Camino Ramón Padilla 2100, Las Agujas, Nextipac, C.P. 45200 Zapopan, Jalisco, México

⁷ Nickel District Conservation Authority (NDCA), 401-199 Larch Street, Sudbury, ON P3E 5P9, Canada

⁸ Marine Geology Division, Iranian National Institute for Oceanography and Atmospheric Science (INIOAS), P.O. Box, Tehran 14155-4781, Iran

impact on the Urmia Lake has led to the drastic present water imbalance (Hassanzadeh et al. 2012; AghaKouchak et al. 2015; Khazaei et al. 2019; Sharifi et al. 2021), natural climate variability and drought have also been invoked as the driving forces behind its rapid decline, a narrative that is particularly favored by the government (Farsnews 2011; Khabaronline News Agency 2011).

One of the challenges in understanding the optimum water input/output requirements for the natural sustainability of Urmia Lake's unique and intricate ecosystem today is the scarcity of long-term (multidecadal to millennial) climate and hydrological baseline data (Sharifi et al. 2018b). Terminal lakes with high salinity levels such as Urmia are sensitive to climate forcing mechanisms and thanks to inhibited bioturbation; their sediments can preserve high-resolution records of abrupt climate variability and environmental change (Fritz 1996). Nevertheless, inorganic precipitation of calcium carbonate in Urmia Lake and carbon contribution from older geological formations in its watershed can complicate the development of a robust age model (Stevens et al. 2012; Talebi et al. 2016).

The first published paleoclimate records from Urmia Lake covered the past 13,200 years and were based on sedimentological (Kelts and Shahrabi 1986) and pollen (Bottema 1986) data from a 4.5-m-long sediment core. This record's chronology was based on extrapolations from two un-calibrated radiocarbon dates derived from *Artemia* fecal pellets. Data from these studies were interpreted to indicate low lake levels from the beginning of the record till about 9000 year BP, high lake levels from 9000 to 7300 year BP, and the predominance of "modern conditions" after 7300 year BP. However, these early attempts to reconstruct Holocene paleoenvironmental conditions at the lake disagreed with lake records from Turkey (Degens et al. 1984) and North Africa (Street-Perrott and Roberts 1983), due to the uncertainties in the chronology of the sediment core as noted by the authors (Kelts and Shahrabi 1986).

The longest paleoclimate record for Urmia Lake is from a 200,000-year climate reconstruction based on pollen and $\delta^{18}\text{O}$ values from a 100-m sediment core (Djamali et al. 2008a; Stevens et al. 2012) collected from the middle part of the lake. The core chronology, which is missing the Holocene period, was established by temporal correlation of the Urmia sediments with other available records from the region and by extrapolation of two calibrated radiocarbon dates on bulk samples. This age model was later improved by six additional U/Th dates on *Artemia* fecal pellets, providing an upper lower limit of 180,000 years (Stevens et al. 2012). Based on this record, the authors concluded that warm and moist climate conditions prevailed during the last penultimate deglacial transition, while the transition from the last glacial to the Holocene was relatively cooler and drier (Djamali et al. 2008a; Stevens et al. 2012). Nevertheless,

the authors were not able to infer the Marine Isotope Stage (MIS) 5-MIS4 transition and climate variability during the Holocene due to sediment loss during coring and imprecise dates.

Recently, Tudryn et al. (2021) attempted to reconstruct climate conditions and the environmental evolution of the lake during the past 30,000 years based on a composite record of magnetic susceptibility, electrical conductivity, and mineralogy obtained from seven cores collected in the vicinity of Shahr Chay river mouth at the western fringe of the lake. The authors identified two major drought events which occurred at ~ 30 and at 5.5–4.9 cal kyr BP and concluded that Urmia Lake experienced several episodes of low stands since the Last Glacial Maximum (LGM). Six radiocarbon dates were used to establish the chronology, though an age model was not provided since the radiocarbon control points were dispersed between three cores with missing intervals resulting from poor sediment recovery.

To address the question of natural versus anthropogenic causes of the abrupt changes in the Urmia Lake's hydrochemical imbalance over the past three decades, a high-resolution record of past hydroclimate variability with a robust chronology is needed. Here, we present a new multi-proxy reconstruction of paleohydrologic changes in Urmia Lake for the past 11,300 years from a 5-m-long sediment core taken from the eastern fringe of the lake in 2012 (Fig. 1). We interpret the geochemical proxies and pollen variability in the context of a well-calibrated chronology with a novel approach to resolving the influence of reservoir carbon ages on radiocarbon dates in bulk sediments, brine shrimp (*Artemia*) cysts, and fecal pellets. We further examine potential atmospheric teleconnections during the Holocene by comparing our results with existing records from the eastern Mediterranean Sea and the North Atlantic.

Study area

The Urmia Lake basin is part of the complicated tectonic zone between the colliding Arabian and Eurasian plates (McKenzie 1972, 1976) and presents a diverse geological setting with a variety of rock formations of different ages, ranging from Precambrian metamorphic complexes to Quaternary mud deposits (Shahrabi 1994; Sharifi et al. 2018b). The lacustrine sediments are comprised of a mixture of chemically precipitated aragonite, shrimp fecal pellet sands, detrital clays, thin aragonite crusts, oolites, and evaporites (gypsum and traces of dolomite around the lake margins) (Shahrabi 1994; Sharifi et al. 2018b).

The climate of the Urmia region is classified as Mediterranean pluvisesonal continental (Rivas-Martinez et al. 1999) with most of the precipitation falling from March to May. Mean annual precipitation for the last 55 years at the

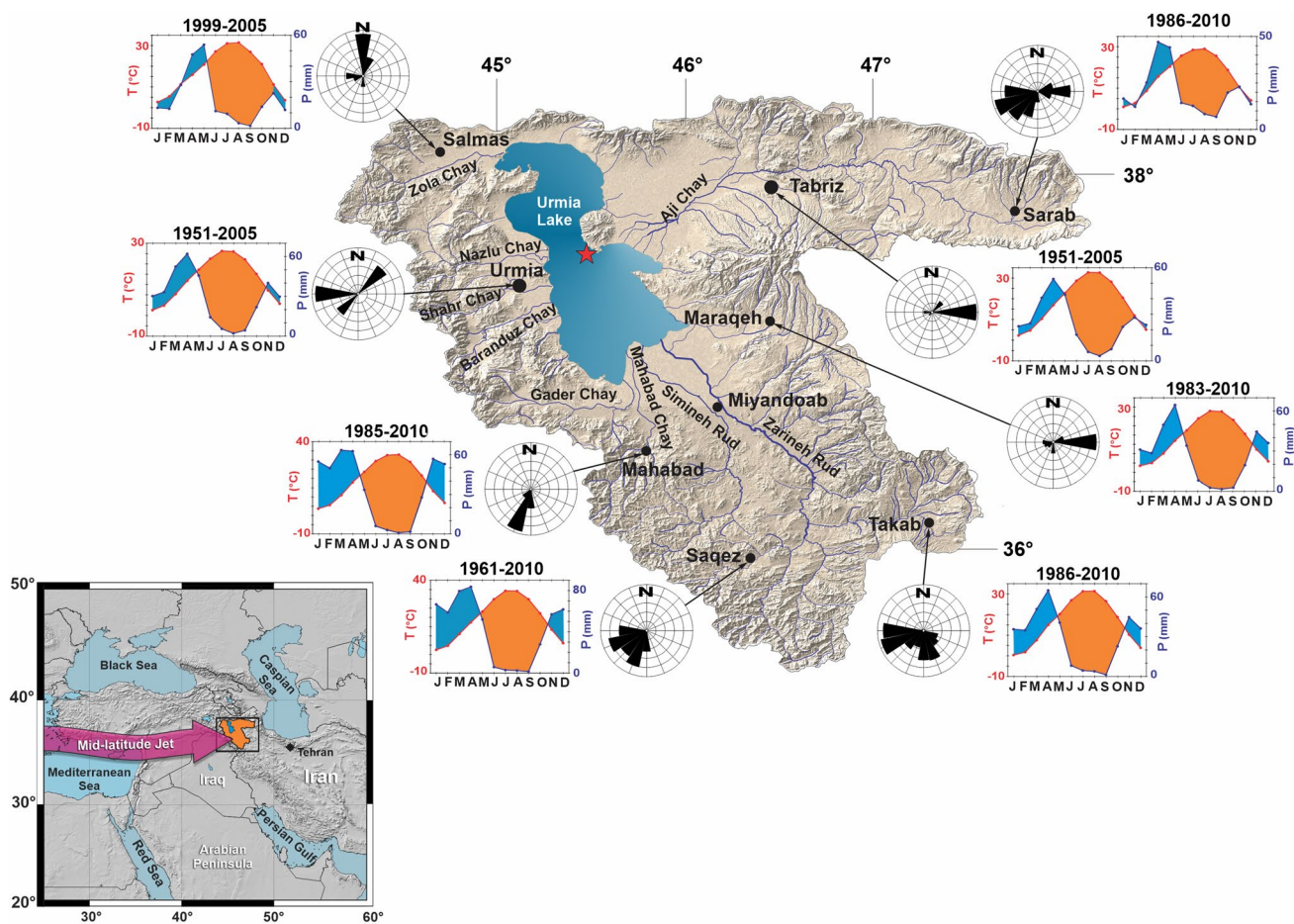


Fig. 1 Location of the Urmia Lake watershed area and major perennial and seasonal tributaries. Climate and rose-wind diagrams denote the long-term average annual maximum temperature, precipitation,

and prevailed wind speed recorded at major meteorological stations (data from the Iran Meteorological Organization, www.imo.ir). Red star denotes the location of the core

Urmia meteorological station (west of Urmia Lake at 1313 m.a.s.l.) is 340 mm. Mean annual temperature recorded at Urmia meteorological station is 11.2 °C, ranging from an average of - 2.5 °C for the coldest month in January to 23.9 °C in the warmest month of July. The average direction of the prevailing winds over the Urmia Lake watershed at stations spanning the last 25 to 50 years is westerly and southwesterly (Fig. 1).

Lake level is controlled by the balance between riverine input and precipitation over the watershed area (52,000 km²), and evaporation estimated to average about 1 m year⁻¹ (Sima et al. 2013), but can increase to 1.5 m year⁻¹ driven by strong NW-SE seasonal winds (Kelts and Shahrabi 1986). Most of the water that flows into the lake is from the Zarrineh Rud and Simineh Rud rivers, both of which discharge to the lake from the south (Fig. 1). The lake is presently divided into two sub-basins separated by a causeway and bridge completed in 2008. The causeway allows for a 1.5-km exchange gap between the northern basin with an average depth of 10 m, and the southern basin with an

average depth of 2 m (Sharifi et al. 2018b). Since 1977, the salinity of the lake has varied from 140 to more than 220 g L⁻¹ on an annual basis, while the average surface area of the lake has ranged between 4750 to 6100 km² (Eimanifar and Mohebbi 2007; Sharifi et al. 2018b). Salinity values exceeding 300 g L⁻¹ have been reported during the latest phase of lake level decline (Rezvantlab and Amrollahi 2011; Sharifi et al. 2018b).

Materials and methods

Sampling

In the summer of 2012, we recovered a 5-m core from the east coast of the Urmia Lake (Fig. 1). A duplicate core (5.4 m) was also obtained 50-cm away from the first core. The coring site has experienced a sever change in water depth due to the rapid desiccation of the lake since 1995. In 2000, the coring site was covered by 2 to 3 m of water. However,

in 2012, the lakebed was fully exposed at the coring location and covered by a 10-cm thick evaporite layer. Half-barrel cores were collected in 1-m increments of 7-cm diameter using a Russian Split Corer. All cores were photographed on site and transferred into pre-cleaned PVC core liners, sealed in non-reactive plastic sheets, and stored at 4 °C. Individual core segments were transferred into an especially-designed polymethyl methacrylate core holder and PVC liner with scale bars. The cores were subsequently imaged using a Geotek Multi-Sensor Core Logger (GeotekMSCL) at the Department of Marine Geosciences (MGS), at the Rosenstiel School of Marine and Atmospheric Science (RSMAS), the University of Miami. Calibration for white balance, light intensity and cross-core resolution was conducted prior to imaging. Down-core XRF elemental intensities and core images were used to determine the position of each sample taken for discrete geochemical analyses. To minimize the effect of aliasing and to capture the entire range of variability, samples were taken from areas of high and low XRF intensities as well as midpoints. Sub-samples were taken using a pre-cleaned ceramic knife and the samples were dried at 45 °C over 5 days.

Age model

To construct a robust radiocarbon age model that accounts for the C-14 reservoir effect of Urmia Lake on bulk samples, we compared the bulk sediment ages from two intervals from the duplicate 5.5-m-long core (Fig. 2 and Table 1) with ages measured on brine shrimp (*Artemia*) fecal pellets and reproductive cysts. Approximately 20 mg of intact fecal pellets and shrimp cyst were collected from two 15-cm intervals at 0.65 and 5.4 m of the sediment core. Shrimp cysts were rinsed in 1 mL of 0.01 M HCl solution followed by 5

mL of MilliQ water (18 mΩ) to remove potential carbonate contamination and were dried in the oven at 40 °C for 4 h. Homogenized bulk samples were also collected from the same intervals. These samples along with 8 other bulk sub-samples were submitted for ¹⁴C dating to Beta Analytic Inc., Miami. Bulk samples were pretreated using acid-only protocol prior to graphitization. No further treatment was conducted on shrimp cysts and fecal pellets. Ages were based on ¹⁴C analysis and associated errors were calibrated using Calib8.2 online platform (Stuiver et al. 2021) by utilizing IntCal20 calibration dataset (Reimer et al. 2020). Since the shrimp cysts contained the most pristine organic content in the Urmia Lake sediment (Djamali et al. 2010b; Manafar et al. 2011), the age difference between the radiocarbon dates driven from shrimp cyst and the ones from the bulk or fecal pellet samples collected from the same interval are the best representation of the “reservoir effect.” Subsequently, all radiocarbon dates were corrected for the reservoir effect prior to calibration and reported as calibrated year before present (cal. yr BP).

Comparative calibrated radiocarbon ages from bulk sediment, shrimp fecal pellet, and shrimp cyst extracted from 0.65- and 5.4-m intervals of the long core from the NE margin of the lake are shown in Fig. 2 and the data are presented in Table 1. Among the collected samples, shrimp cyst was of the youngest age. By averaging the age difference between shrimp cyst calibrated radiocarbon dates and the ones from bulk sediment and fecal pellet samples at 0.65- and 5.4-m intervals, we considered a 560- and 719-year correction on bulk sediment and fecal pellets radiocarbon dates, respectively to account for the Urmia Lake’s reservoir effect. Age-depth model was constructed based on a Bayesian approach in “Bchron” package (Hallett and Parnell 2008; Parnell et al. 2008) (Fig. 3). The

Fig. 2 Comparative calibrated AMS radiocarbon ages measured on bulk sediment, shrimp fecal pellets, and *Artemia* cyst at two different depths from Urmia Lake. The average age offset between bulk sample and cyst is considered the reservoir effect correction factor (see text for details)

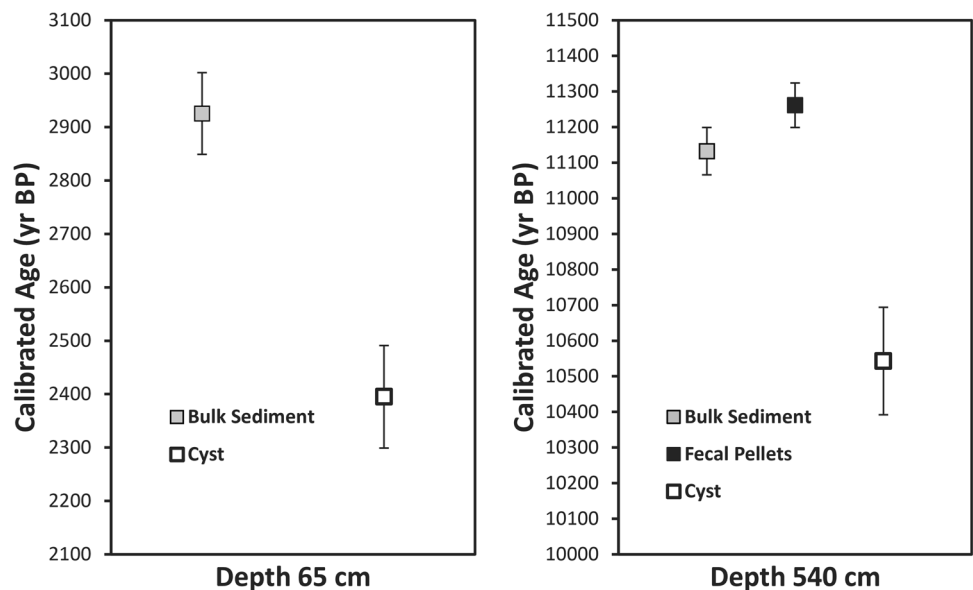


Table 1 Radiocarbon dates and calibrated ages corrected for reservoir effect

Sample no.	Depth \pm 5 mm*	Sample type	Conventional age (RCYBP) \pm reported uncertainty**	Midpoint calibrated age (year BP) \pm 2 σ error	Median calibrated age (BP) corrected for reservoir effect***	Calibrated 2 σ age range (BP)
U7-2B	640	Bulk sediment	2820 \pm 30	2926 \pm 77	-	-
U7-2C	640	Cyst	2330 \pm 50	2395 \pm 96	-	-
U7-2f	5400	Fecal pellets	9850 \pm 40	11,262 \pm 63	-	-
U7-2c	5400	Cyst	9330 \pm 50	10,543 \pm 151	-	-
U7-2b	5400	Bulk sediment	9660 \pm 40	11,133 \pm 67	-	-
U6-1-3	35	Bulk sediment	680 \pm 30	-	113	9–151
U6-1-2BK	111	Bulk sediment	1860 \pm 30	-	1228	1176–1289
U6-1-1BK	487	Bulk sediment	2690 \pm 30	-	2098	1199–2153
U6-2-3	1005	Bulk sediment	4890 \pm 30	-	4893	4841–4967
U6-2-2BK	1390	Bulk sediment	5130 \pm 40	-	5248	5051–5193
U6-3-3BK	2328	Bulk sediment	7610 \pm 40	-	7883	7790–7963
U6-4-4BK	3312	Bulk sediment	9580 \pm 50	-	10,200	1011–10,252
U6-5-5BK	4571	Bulk sediment	10270 \pm 40	-	11,155	11,072–11,234

* Indicates the error on depth measurement

** RCYP, radiocarbon year before present, for error calculation please refer to the information provided by Beta Analytic Co. on radiocarbon data and calculation protocol at <http://www.radiocarbon.com>

*** Calibrated ages were corrected for the reservoir effect by 560 years prior to calibration. The 560-year correction is based on the age difference between comparative bulk sediment and shrimp cyst. All corrected ages recalculated for present time being 2012

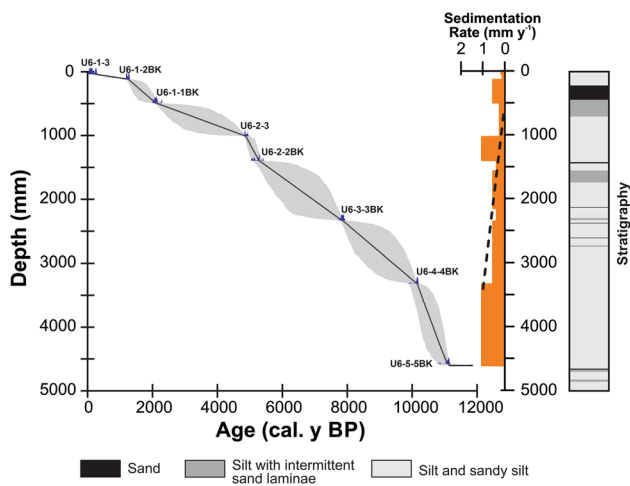


Fig. 3 The Bayesian age model for the Urmia Lake sediment core based on 8 calibrated AMS radiocarbon dates is shown (see Table 1 for details). The gray area between tie points refers to the 2 σ uncertainty. Bayesian sedimentation rates (SR) between paired tie points are shown on the right axis. Dashed black line denotes the overall SR trend since the beginning of the record at 11,620 cal. y BP. All ages are corrected for reservoir effect. Simplified stratigraphy of the core is shown on the right

code was run using R version 3.5.3 (Team Rs 2015). We used the “sedimentation rate” output field in “Bchron” to create sedimentation rates for the sediment core (Fig. 3) (see Table 1 for the data).

Major and trace element analysis by XRF scanning

High-resolution measurements of the relative abundances of trace and major elements were performed on an AVAAT-ECH XRF-core scanner in the Palaeoclimatology Lab at RSMAS-MGS. All core sections were scanned twice (10 kV, 1000 μ A, no filter; 30 kV, 1000 μ A, Pd filter) to acquire the range of elements reported here. For all measurements, the surface area was irradiated for 20 s of integration time at 1-mm intervals (an average sampling resolution of 2.3 years) using a window 1 mm high by 12 mm wide for the lake sediment cores. The raw XRF spectra were then processed using the Canberra WinAxil software with standard software settings and spectrum-fit models, and abundances are reported as the intensity of each element in counts per second (cps). The JR-1 standard (Geological Survey of Japan) was used for calibration, and calibrated data were compared with previous measurements to check for discrepancies. The down-core XRF elemental abundances are interpreted as a qualitative proxy for changes in sediment load to the lake throughout the core (see Dataset S1 for XRF data).

Elemental analysis

To quantify the XRF results and to calculate variation in weathering indices over the last 11,300 years, 68 samples (average sampling resolution of \sim 165 years) were collected for analysis of major oxides. Approximately 1 g of dried and homogenized sample was transferred

to 50-mL centrifuge tube and rinsed with MilliQ water (18 mΩ) following sequential stages of 30-min agitation, 30-s sonication, and 20-min centrifuging at 3500 rpm. The dried sample was transferred to capped, high-purity quartz crucibles, and ashed in a muffle furnace at 750 °C for 1 h to remove organic materials. A 20-mL solution of 1 M NaAc in 25% HAc (final pH = 4) was added to the organic-free sample in a 50-mL centrifuge vial and continuously agitated for 2 h at room temperature to remove the carbonate content. Samples were centrifuged at 5000 rpm for 15 min and the supernatant solution was discarded. This stage was repeated until no fizzing/bubbling was visible. The sample was rinsed with MilliQ water (18 mΩ) twice and oven dried at 60 °C overnight. Approximately 0.01–0.02 g of organic and carbonate free sample was transferred to a pre-cleaned 6-mL PFA Savillex vial and dissolved in 5 mL of concentrated HNO₃-HCl-HF mixture (2:2:1, volumetric ratios) following the method described by Sharifi et al. (2015). After complete digestion was achieved, about 0.1 g of the solution was diluted in 40 g of 0.45 mol L⁻¹ HNO₃ and elemental concentrations was measured against a multi-elemental standard solution (Spex CertiPrep) of known concentration (± 5%) by sample-standard-sample bracketing technique on the multi-collector inductively coupled plasma mass spectrometer (MC-ICP-MS) at the Neptune Isotope Laboratory (NIL), RSMAS. Elemental concentrations were reported as percentage of oxides. The accuracy and precision of measurements were evaluated by comparing analyses of USGS certified reference material BHVO-2 with literature compilations (GEOREM, <http://georem.mpch-mainz.gwdg.de/>). Results for reference materials agreed well with literature values within analytical uncertainties (Fig. S-1). Contributions from the procedural blank were negligible (smaller than 0.1%).

Paleo-precipitation reconstruction

Variations in weathering indices as proxies for the supply of weathered material to marine and lacustrine environments have been employed to study changes in the hydrologic regime of depositional basins (Sheldon et al. 2002; Myers et al. 2014; Harmon et al. 2016). A widely utilized weathering index to estimate rainfall is CIA-K, which is similar to the chemical index of alteration (CIA) (Nesbitt and Young 1982, 1989) minus potassium to account for the potential effect of illite formation which leads to potassium enrichment in sediment (K-metasomatism) (Meunier et al. 2013; Myers et al. 2014). The CIA-K is calculated based on molar values of oxides and expressed as follows:

$$\text{CIA} = 100 \times [\text{Al}_2\text{O}_3 / (\text{Al}_2\text{O}_3 + \text{CaO}^* + \text{Na}_2\text{O})] \quad (1)$$

where CaO* is CaO associated with the silicate fraction of the sample. Results of elemental analysis conducted on 68 samples were converted to molar values of oxides and used to calculate the downcore variation of CIA-K.

Several studies have shown a correlation between the amount of rainfall and degree of weathering (Sheldon et al. 2002; Nordt and Driese 2010; Myers et al. 2014), making it possible to empirically estimate mean annual precipitation (MAP) with the use of weathering indices. Specifically, the MAP estimates based on a CIA-K weathering index are used to discriminate soil types with various clay contents (vertic and non-vertic soils) as shown in Eqs. (2) (Sheldon et al. 2002) and (3) (Nordt and Driese 2010):

$$\text{MAP}(\text{mmy}^{-1}) = (14.3 \times \text{CIA} - \text{K}) - 37.6, R^2 = 0.73 \quad (2)$$

$$\text{MAP}(\text{mmy}^{-1}) = (18.64 \times \text{CIA} - \text{K}) - 350.4, R^2 = 0.81 \quad (3)$$

Wavelet analysis

To identify the major periodicities within the time series used in this study, wavelet power spectrum analyses were performed on downcore variations of Al abundances, North Atlantic Holocene Ice Rafted Debris (IRD) events (Bond et al. 2001, 1997), and 11 ka reconstruction of sunspot numbers based on ¹⁰Be (Solanki et al. 2004) time series using the Morlet wave (Torrence and Compo 1995) and a modified MATLAB script. Prior to the analysis, each time series was detrended and linearly interpolated to create an equally spaced time series. To detrend the time series, the least-square best-fit line was subtracted from the original data by using the built-in MATLAB command.

Pollen extraction, identification, and illustration Pollen analysis

Pollen samples were taken with 5-cm sampling intervals (average sampling resolution of ~ 245 year) along the core. The samples, each with 2 cm³ volume, were then weighed and treated following a modified version of Moore et al. (1991). Highly soluble salts were first removed by rinsing with distilled water followed by centrifuging at 2500 rpm for 7 min. One lycopodium tablet (Batch No. 1031) was then added to each sample to calculate pollen concentrations (Stockmarr 1971). Successive treatment with 10% HCl, 48% HF, and 37% HCl were then applied to remove carbonates and evaporites. In some cases, many microcrystals formed after the HCl/HF treatment and a second treatment with 48% HF and 37% HCl was needed to completely remove this secondary byproduct. After the acetolysis, the samples were

filtered between 160 μm and 10 μm and mounted on slides for microscopic identifications under $\times 500$ magnification. Pollen identifications were assisted by using the Mediterranean and SW Asian pollen reference collection hosted in Institut Méditerranéen de Biodiversité et d'Ecologie but also printed pollen atlases of Reille (1992, 1995, 1998), Beug (2004), and Van Zeist and Bottema (1977). Pollen morphological "types" are defined based on Beug (2004) for most of the taxa and on van Zeist and Bottema (1977) for some specific pollen taxa of the Irano-Turanian region (e.g., *Atraphaxis* and *Cousinia*).

Pollen percentages were calculated using TILIA and the pollen diagrams were created in TGView software (Grimm 1992). Amaranthaceae and aquatic pollen (e.g., Cyperaceae and Sparganium-type) were excluded to calculate the pollen sum of terrestrial plants. Amaranthaceae were excluded because this family is dominating the saline soils and salt flats around the lake with a huge pollen production masking the visibility of the variations of terrestrial pollen (Djamali et al. 2008b).

Results

The results from visual inspection of the sedimentary sequences deposited in the area of the lake the cores were taken from are shown in Fig. 3. The detailed description of the sedimentary sequence was also presented in the supplementary materials (Core logs). The core was mainly composed of silt, sand, and silt with intermittent sand intervals. The thickness of sand layers varied from 20 cm at the top to 5 mm throughout the rest of the sequence. These sand intervals were more frequent at the top half of the sequence (Fig. 3) and can be easily traced between the collected cores. *Artemia* fecal pellet appears the main component of the silt and sandy silt layers. Most significantly, there were no visible evaporative horizons anywhere along the entirety of the core.

To construct a robust radiocarbon age model that accounts for the C-14 reservoir effect of Urmia Lake on bulk samples, we compared the bulk sediment ages from two intervals along the 5.4-m-long core (Fig. 2 and Table 1) with ages measured on brine shrimp (*Artemia*) fecal pellets and reproductive cysts. Among the analyzed samples, *Artemia* cysts were of youngest. The average age difference between *Artemia* cyst calibrated radiocarbon dates and the dates from bulk sediment and fecal pellet samples through the record suggest a 560- and 719-year offset between bulk sediments and fecal pellets, respectively. The resulting Bayesian age model based on 8 calibrated radiocarbon dates is shown in Fig. 3 (see Table 1 for the data). The minimum and maximum sedimentation rates (SR) calculated based on

the Bayesian age-depth model were 0.07 and 1 mm year^{-1} respectively, with the overall decreasing trend from the Early Holocene to the Late Holocene.

To investigate processes that provide insight into the dominant climate regime of the record, down-core abundances of conservative lithogenic, redox sensitive, and mobile elements were measured by XRF scanning at 1-mm intervals (an average resolution of 2.3 years). This was accompanied by discrete elemental analyses on 68 samples (average resolution of ~ 165 years) by MC-ICP-MS. These data are shown in Figs. 4 and 6 (see Datasets S1 for data). Aluminum and Si intensities show at least 10 periods that contributed elevated levels of aluminosilicate minerals since 11,300 years BP (Fig. 4a and b). From the beginning of the records, these episodes can be constrained between the following periods: 11,100–10,500, 10,450–9700, 9650–9100, 8400–7100, 6500–5850, 4100–3200, 3050–2600, 2550–1850, 1450–500, and 300–50 years BP. The Al-normalized ratios of conservative lithogenic elements (Si/Al, Ti/Al, and Zr/Al) are interpreted as proxies for aeolian input (Calvert and Pedersen 2007; Nieto-Moreno et al. 2011; Govin et al. 2012; Jiménez-Espejo et al. 2014). As shown in Fig. 4d–f, these ratios covary throughout the entire record, with increased variability and abundances towards the Late Holocene. At least 13 episodes with high Si/Al, Ti/Al, and Zr/Al ratios were identified since the beginning of the record which ranged from 11,200 to 11,000 BP, 10,700 to 10,300 BP, 9900 to 9600 BP, 9150 to 8950 BP, 7700 to 7400 BP, 7000 to 6500 BP, 6000 to 5500 BP, 4400 to 3950 BP, 3200 to 2900 BP, 2700 to 2300 BP, 2100 to 1500 BP, and 200 BP to present.

Considering that K is more readily mobilized than Rb during chemical weathering (Muhs et al. 2001; Brown 2011), we assess the intensity of chemical weathering and river input to the lake using the variations in Rb/K ratios in the sediment (Fig. 4g). The Mn/Al ratio is used as a proxy to track changes in the redox state of the sediment horizon. Variations in Fe (Fig. 4h and i) are used to demonstrate fluctuations in bottom water oxygen levels at the time of sediment deposition (Calvert and Pedersen 2007; Rodrigo-Gámiz et al. 2014; Martínez-Ruiz et al. 2015). In comparison, high Rb/K ratios can be observed to coincide with the episodes of higher Mn/Al ratios and lower abundances of Fe (Fig. 4g–i). Lake-level fluctuation inferred from Si/Al, Ti/Al, Zr/Al, Rb/K, and Mn/Al ratios as well as from downcore abundances of Fe is presented as high and low intervals in Fig. 4h (see Discussion for details). The episodes of low lake level are more frequent during the Mid- to Late-Holocene and ranging from 11,150 to 11,000 BP, 10,600 to 10,350 BP, 9800 to 9600 BP, 9150 to 8350 BP, 7000 to 6450 BP, 5950 to 5450 BP, 5300 to 4750 BP, 4400 to 4000 BP, 3850 to 3600 BP, 3200 to 3000 BP, 2700 to 2550 BP, 2400 to 2300 BP, 2100 to 1400 BP, 1350 to 1250 BP, 900 to 300, and 200 BP to present. Paleorainfall ($\text{MAP}_{\text{paleo}}$) reconstructions

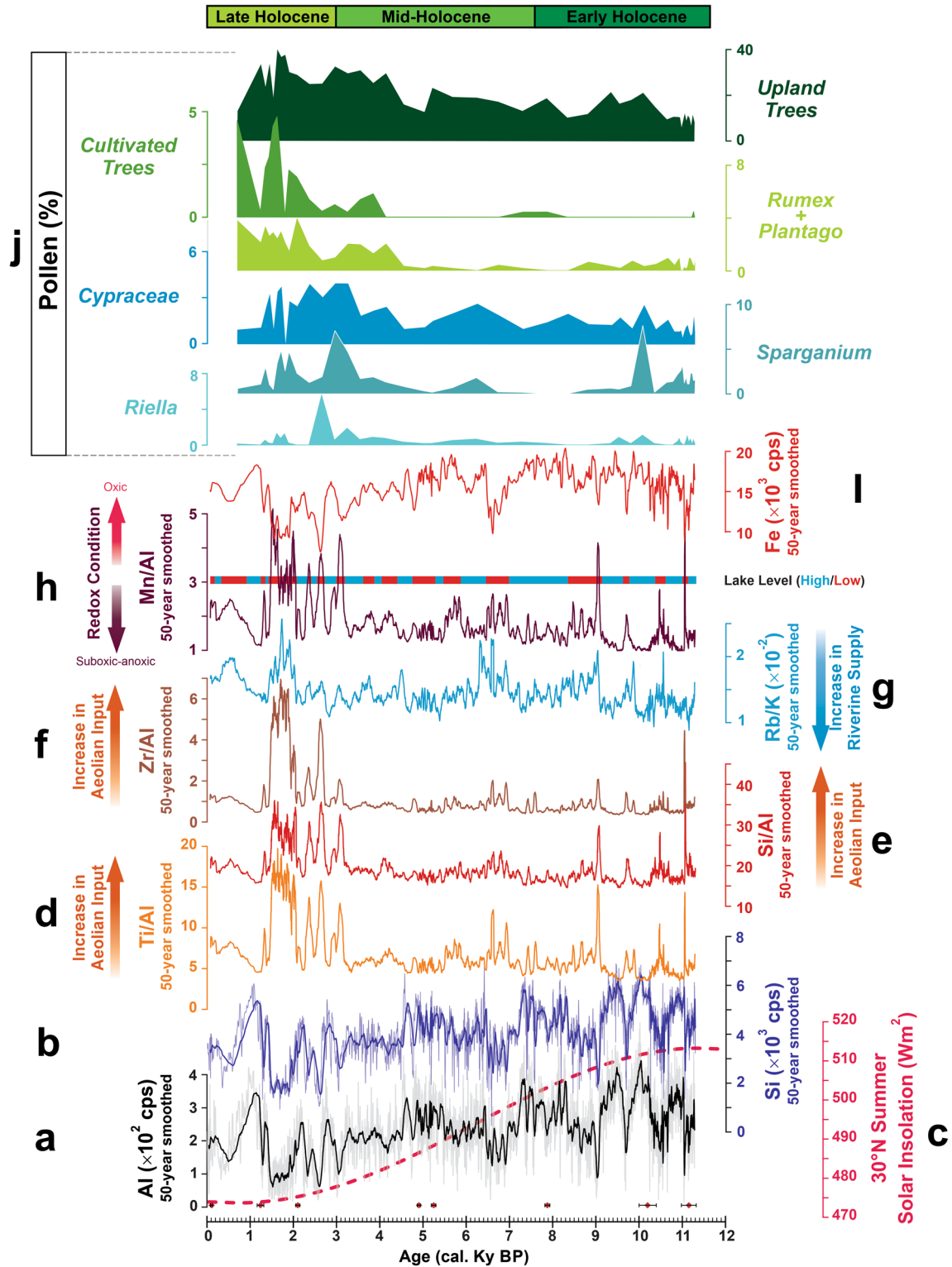


Fig. 4 Multi-proxy sediment record in Urmia Lake from NW Iran. (a and b) 50-year smoothed scanning XRF intensity profile for Al ($\times 10^2$ cps) and Si ($\times 10^3$ cps) respectively, original data are shown in grey and pale blue, 8 radiocarbon dates (filled diamonds), and their associated uncertainties (2σ) are plotted along the age axis. (c) Summer solar insolation (Wm^{-2}) at 30°N. (d–f) Down-core profiles of the Al-normalized abundances of lithogenic (Ti, Si, Zr) elements used as

aeolian input proxies. (g) Rb/K ratio ($\times 10^{-2}$) as proxy for riverine input and weathering. (h–i) Al-normalized abundances of Mn as well as down-core XRF intensity profile of Fe ($\times 10^3$ cps) as paleoredox proxies. The blue/red bars are referred to high/low lake levels inferred from geochemical proxies (see text for more details). (j) Pollen accumulative percent

based on the Eqs. (2), (3), and (4) revealed four major low precipitation events centered at 8400 BP, 3100 BP, 1500 BP, and 800 BP. These episodes are well correlated with the episodes of low lake levels inferred from geochemical proxies (Fig. 6a and b) (see Discussion for details).

Pollen percentages were calculated based on the total pollen sum (aquatic + terrestrial pollen) for wetland pollen types, and on pollen sum (terrestrial pollen excluding aquatic pollen) for upland plants including anthropogenic pollen indicators. Pollen types were assigned into four ecological groups: Irano-Anatolian upland types (deciduous trees + junipers), wetland types (Cyperaceae, *Sparganium*-type, and *Riella*), agro-pastoral indicators (*Cerealia*-type pollen, *Plantago lanceolata*-type, and *Rumex*), and indicators of well-established sedentism and urban development (cultivated trees) (Fig. 4j). Tree pollen percentage variations suggest that the expansion of forests (upland trees in Fig. 4j) following deglaciation occurred slowly. Indeed, the Zagros-Anti Taurus deciduous woodlands were established between 7000 and 6000 years BP (Djamali et al. 2010a). Agro-pastoral pollen indicators have been present since the beginning of the Holocene. However, their abundances start increasing after roughly 5000 years BP, a trend that continues until the end of the record. The pollen indicators of true sedentism and urbanism and true sedentism (e.g., cultivated trees) also start increasing after about 4200 years BP, with maximum values during time intervals centered between 1700 and 1400 years BP, and a final peak at 700 years BP.

Discussion

Major and trace element proxies

Distinctive hydrological shifts in Urmia Lake basin, especially during the Last Glacial Maximum, resulted in deposition of distinctive evaporite-rich layers (Shah-Hosseini 2003; Stevens et al. 2012). However, without visible evaporite horizons in our 5-m-long sediment core, we instead use down-core elemental abundances to identify periods of potential hydrological imbalance during the past 11,300 years.

It has been shown that the supply of aeolian input into marine and lake environments increases during dry periods (Harrison et al. 2001). Studies of dust emission and transport in West Asia during both the Holocene (Sharifi et al. 2015, 2018a) and the modern era (Middleton 1986; Prospero et al. 2002) further confirm higher dust transport and deposition to the region and to where the lake is located during dry periods. Higher concentration of aeolian particles in lake sediment can increase the concentrations of Si, Ti, and Zr, leading to an increase in the Al-normalized values (Si/Al, Ti/Al, and Zr/Al) (Calvert

and Pedersen 2007; Nieto-Moreno et al. 2011; Govin et al. 2012; Jiménez-Espejo et al. 2014). It worth mentioning that the elements transported to the Urmia Lake by the rivers represent the elemental input averaged over 52,000 km² watershed area with less fluctuated elemental ratios. Therefore, Si/Al, Ti/Al, and Zr/Al variability must be considered as the relative contribution of aeolian versus fluvial input (Lourens et al. 2001).

As such, it can be argued that changes in the supply of wind-blown dust can be interpreted as episodes of dry climatic condition (Martinez-Ruiz et al. 2015). The most compelling evidence that high Si/Al, Ti/Al, and Zr/Al ratios in the Urmia Lake core represent dry periods of erosion and enhanced aeolian input is the observation that these periods coincide with intervals of low abundances in Al intensities (compare panels d, e, and f to a in Fig. 4).

Considering the behavior of mobile elements such as Rb and K in riverine systems during dry conditions (transport-limited denudation) versus humid periods (weathering-limited denudation), sediments with high Rb/K ratios are indicative of dry periods during which low riverine fluxes are expected (Stallard 1985; Brown 2011). Several episodes of high Rb/K ratios in the Urmia Lake core coincide with intervals of high Si/Al, Ti/Al, and Zr/Al ratios (Fig. 4 d–g), indicating higher aeolian input during times of low riverine fluxes that likely were accompanied by dry spells over the catchment basin.

Under oxygenated conditions, Mn forms highly insoluble Mn (III) or Mn (IV) oxi-hydroxides that are rapidly deposited in particulate form. Conversely, under anoxic conditions, Mn is reduced to Mn (II) and forms soluble Mn²⁺ or MnCl⁺ cations that diffuse out of the sediment, or from the sediment-water interface into the water column (Calvert and Pedersen 1993; Algeo and Maynard 2004). This behavior of Mn is expected to result in high (low) Mn/Al ratios during oxic (suboxic-anoxic) condition (Rodrigo-Gámiz et al. 2014; Martinez-Ruiz et al. 2015).

Down-core variations of Mn/Al ratios in the sediment core (Fig. 4h) indicate several intervals of elevated ratios, indicative of higher oxygen conditions at the sediment-water interface. These periods are associated with low Fe abundances along the core (Fig. 4i). The relationship between sediment Mn and Fe contents and oxic-anoxic conditions is not always straightforward and factors such as water column sulfur content, total organic content, biomineralization of Mn- and Fe-bearing minerals, and the stratification of the water column with respect to oxygen and circulation of lake bottom water can play a major role in the final concentration of these redox sensitive elements in the sediment (Miot et al. 2016). In the absence of such information for the Urmia Lake environment, we speculate that the high Fe abundances associated with low ratios of Mn/Al (suboxic-anoxic condition) and Rb/K (high riverine supply) may represent higher lake levels (Fig. 4h).

The lake-level fluctuations inferred from geochemical proxies revealed that during the Early-Mid-Holocene, when solar insolation was higher relative to the Late Holocene (Fig. 4c), high lake levels were sustained for longer periods (Fig. 4h). However, the periods of high lake level became shorter, and the frequency of dry periods increased as solar insolation was reduced from the Mid- to Late Holocene (Fig. 4c and h). This observation correlates well with multi-proxy records from Lake Van (Wick et al. 2003) and Neor Lake (Sharifi et al. 2015), ~ 230 km west and ~ 290 km east of Urmia Lake, respectively. Both lake records suggest higher moisture availability during the Early and Mid-Holocene, with dry conditions more prevalent during the Late Holocene. In the Urmia Lake record, the Late Holocene is marked by increases in aeolian input (high Ti/Al, Si/Al, and Zr/Al ratios), attributed to low lake levels (high Mn/Al ratio), which is also in good agreement with episodes of enhanced aeolian input to Neor Lake and increased aridity at Lake Van (Wick et al. 2003; Sharifi et al. 2015).

Paleo-precipitation

The empirical equations for MAP (Eq. (2) and Eq. (3)) are subject to local environmental conditions such as sediment clay content, the MAP range, vegetation coverage, and the topography of the study area. Therefore, a new empirical equation tailored for the Urmia Lake watershed area and its precipitation range had to be established. By extrapolating the age model, we compared the mean annual precipitation data (1951–2005) recorded at Urmia station with the four elemental discrete analyses from the top 20 mm of the core (Fig. 5). A CIA-K-MAP correlation of $R^2 = 0.99$ was established for the Urmia Lake region (Fig. 5) and Eqs. (2) and (3) were modified as follows:

$$\text{MAP}(\text{mm y}^{-1}) = (4.5092 \times \text{CIA} - \text{K}) + 132.4, R^2 = 0.98 \quad (4)$$

It should be noted that our approach to providing this calibration is based on a small dataset and is subject to improvement as more data from the lake becomes available in future studies. Nevertheless, this is the first attempt to provide an estimate of this kind for past precipitation in the Urmia Lake watershed area. While a more representative calibration model will improve the absolute values of estimated precipitation, the pattern of change in precipitation rate through time should remain valid regardless of what calibration is used.

The CIA-K index was calculated based on 68 discrete samples measured by MC-ICP-MS (average resolution of ~ 165 years) and was used to reconstruct the paleorainfall ($\text{MAP}_{\text{paleo}}$) for the Urmia Lake basin (solid dark blue line in Fig. 6b). As it can be seen in Fig. 6b, regardless of the offset in reconstructed absolute $\text{MAP}_{\text{paleo}}$ values using Eq.

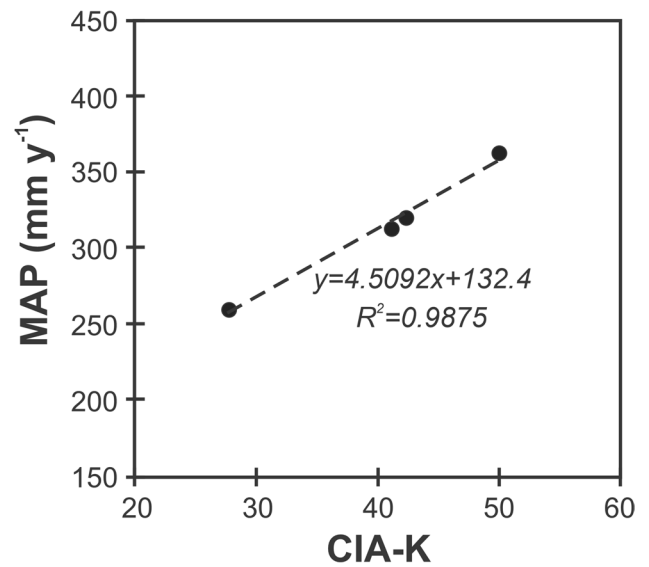


Fig. 5 Relationship between mean annual precipitation (MAP) and CIA-K in samples from Urmia Lake

(2) (upper limit) and Eq. (3) (lower limit), there is good agreement between the mean precipitation patterns throughout the record. Equation (4) returned minimum and maximum $\text{MAP}_{\text{paleo}}$ estimates of 174 mm year⁻¹ and 401 mm year⁻¹, respectively. The $\text{MAP}_{\text{paleo}}$ estimates for the Holocene reveals multiple episodes of low precipitation since the beginning of the record, where the major drops in precipitation are centered at 8400 BP, 3100 BP, 1500 BP, and 800 BP. The average precipitation for the Early Holocene is estimated around 339 mm year⁻¹ while this average reduced to 305 mm year⁻¹ and 287 mm year⁻¹ for the Mid- and Early Holocene, respectively. Considering the difference between the resolution of the $\text{MAP}_{\text{paleo}}$ reconstruction and that of the elemental ratios, the paleo-precipitation reconstruction and lake-level fluctuations inferred from geochemical proxies are in good agreement (Fig. 6 a and b).

The average estimated rainfall for the Holocene shows a decreasing trend from Early to Late Holocene (Fig. 6b), following the decline in summer solar insolation (Fig. 4c), which is in good agreement with down-core abundances of Al (Fig. 4a) and other proxies for redox, aeolian input, and riverine supply (Fig. 4) as discussed above. A correlation between solar insolation and precipitation in the Middle East was previously reported in a cave record from central-west Iran (Mehterian et al. 2017). The observed trend in rainfall estimates is also in good agreement with the multi-proxy record from Neor Lake, where Sharifi et al. (2015) reconstructed the Holocene moisture availability based on variations in a precipitation (Paq) biomarker (Fig. 6c) and δD values of C₂₈ n-alkanoic acid. The paleorainfall ($\text{MAP}_{\text{paleo}}$) reconstruction for the Urmia Lake is also in good agreement with the episodes of wet/dry condition in Neor Lake based

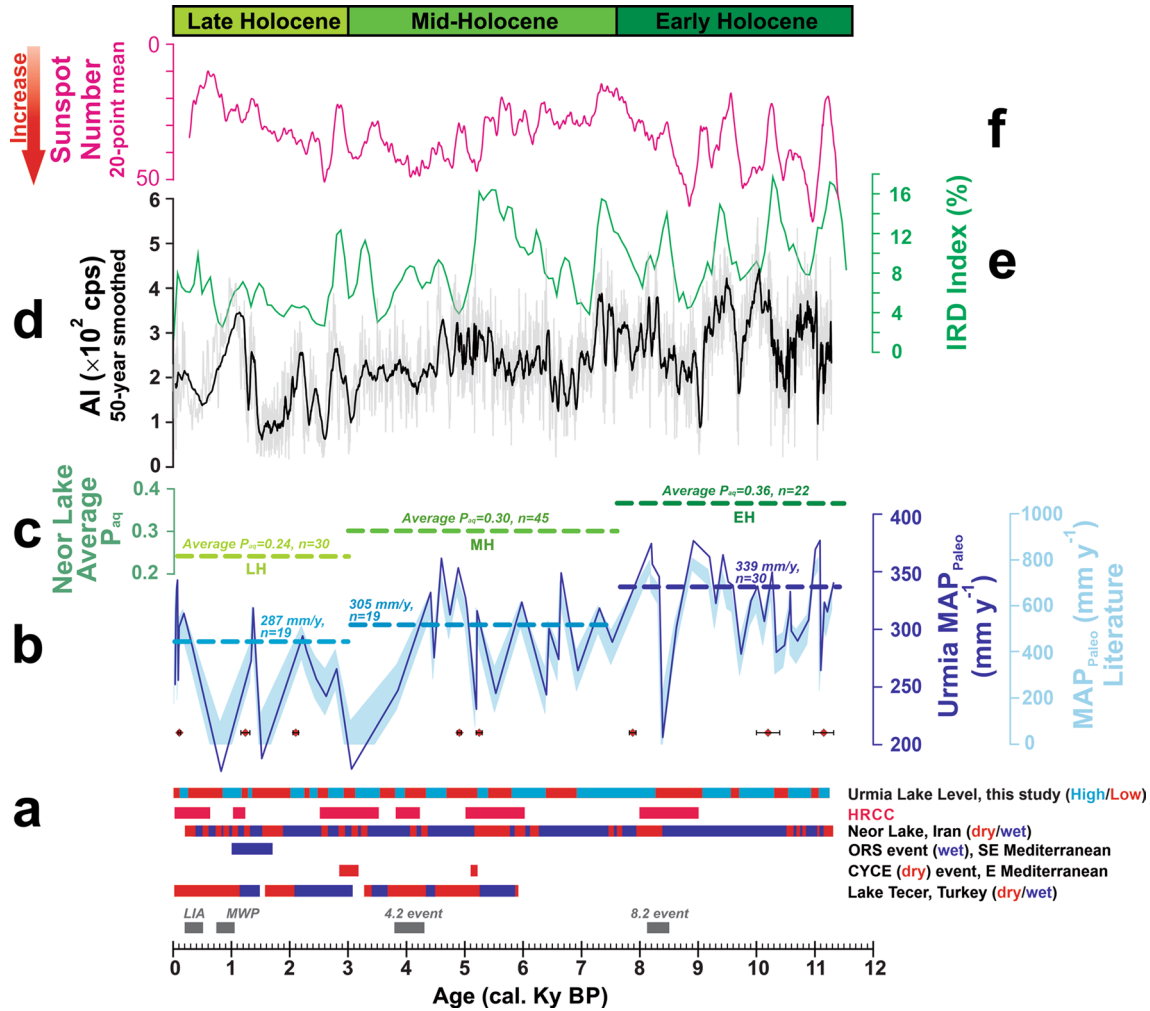


Fig. 6 Paleorainfall reconstruction over Urmia Lake's region. (a) Compilation of paleoclimate records from east Mediterranean (Kaniewski et al. 2019); southeast Mediterranean (Schilman et al. 2001); Lake Tecer in Turkey (Kuzucuoglu et al. 2011); and Neor Lake in northwest Iran (Sharifi et al. 2015). Bars in magenta denote Holocene rapid climate change events (HRCC) (Mayewski et al. 2004). The Urmia Lake level fluctuation (this study) is the same as in Fig. 4. The grey bars are corresponding to 8.2 and 4.2 events, Medieval Warm Period (MWP) and Little Ice Age (LIA). (b) Mean annual precipitation (MAP, mm y^{-1}) estimates based on CIA-K weathering index. Solid dark blue line shows $\text{MAP}_{\text{paleo}}$ reconstruction based on 1951–2005 mean annual precipitation data recorded at Urmia syn-

on downcore variations of Ti (Fig. 6a). This reduction in precipitation from the Early to Late Holocene is also observed in the Holocene record from Lake Van (Wick et al. 2003) as well as in records from the eastern Mediterranean Sea (Schilman et al. 2001; Migowski et al. 2006; Kaniewski et al. 2010). The paleorainfall ($\text{MAP}_{\text{paleo}}$) estimates for Urmia Lake suggest multiple major drops in precipitation during 8.2 and 4.2 events, at 3.1 ka and 1.5 ka, as well as during the Medieval Warm Period and little Ice Age (Fig. 6b). These drops in precipitation over the Urmia watershed area are in

optic station. The light blue-shaded area denotes the $\text{MAP}_{\text{paleo}}$ reconstruction based on equation suggested by Sheldon et al. (2002) (upper limit) and Nordt and Driese 2010 (lower limit), dashed lines denote the average estimated rainfall for the Early, Mid-, and Late Holocene. The age controlling tie points are the same as Fig. 4a. (c) The Neor Lake average P_{aq} index (Sharifi et al. 2015) during Early (EH), Middle (MH), and Late Holocene (LH). (d) 50-year smoothed scanning XRF intensity profile for AI ($\times 10^2$ cps), same as Fig. 4 a. (e) North Atlantic Holocene Ice Rafted Debris (IRD) events (Bond et al. 2001, 1997). (f) 11 ka reconstruction of sunspot numbers based on ^{10}Be , note the vertical axis is in reverse order (Solanki et al. 2004)

good agreement with the global records of Holocene Rapid Climate Change events (HRCC) (Mayewski et al. 2004), the Crisis Years Cooling Event (CYCE) in east Mediterranean (Kaniewski et al. 2019), the dry periods in Lake Neor in NW Iran (Sharifi et al. 2015), and dry periods in Lake Tecer, Turkey (Kuzucuoglu et al. 2011) (Fig. 6a). High paleorainfall ($\text{MAP}_{\text{paleo}}$) estimates are also in good agreement with the wet periods recorded at Neor Lake in NW Iran, Lake Tecer in Turkey, and the Organic Rich Sediment event (ORS) (Schilman et al. 2001) in southeast Mediterranean (Fig. 6a).

Paleo-vegetation

Pollen investigations from Urmia Lake have proven informative in reconstructing (i) regional vegetation changes related to climatic changes (Bottema 1986; Djamali et al. 2008a) and (ii) wetland extension related to lake-level changes (Djamali et al. 2008b; Talebi et al. 2016). Furthermore, anthropogenic pollen indicators have provided insight into the intensity of agro-pastoral activities, lifestyle changes, and urban development in the Irano-Anatolian plateau including the Urmia Lake region (Bottema 1986; Bottema and Woldring 1990; Guibal et al. 2014; Djamali et al. 2016). A comparison of temporal variations of the pollen indicators of upland vegetation, anthropogenic activities, and lake-level changes with geochemical signals provide additional support for the hydrological transition in the lake basin during the current interglacial period.

The Early to Mid-Holocene was characterized by relatively constant lake levels. This observation from the geochemical data is further corroborated by relatively constant values of aquatic pollen during this period (Fig. 6j). The inferred dry phases from 3100 to 1500 years BP marked by frequent episodes of dust input are also characterized by significant fluctuations of pollen abundances of different upland and wetland plants. An important implication of these fluctuations is that they mostly support variations in Ti/Al, Zr/Al, and Mn/Al as a record of hydroclimate changes, and cannot be explained, at least exclusively, by erosion-related events rising from intensified agro-pastoral activities as they may also be indicative of aeolian input. More data will be required to establish each mechanism's contribution to the elemental input to the lake. These wetland pollen types (*Cyperaceae*, *Sparganium*-type, and *Riella*) show the extension of the wetland areas surrounding the lake especially at the fluvio-deltaic environments at the entrance of the incoming river systems (Djamali et al. 2008b). Their increase is thus independent of human activities and provides a direct ecological proxy for lake-level variations. We note that peaks in the abundances of these pollens are out of phase with those of the aeolian intensity peaks, further suggesting that the 3100- to 1500-year BP period was characterized by higher-frequency hydroclimate fluctuations. The lower resolution of pollen record (average sampling resolution of ~ 245 year), however, impedes a direct peak-to-peak comparison with geochemical records.

Another noteworthy observation is that the intensification of sedentary life and development of urbanism as reflected in the pollen curve of cultivated trees shows a continuously increasing trend since the Iron Age with peaks that correspond to the short intervals of higher moisture availability within the 3100- to 1500-year BP time period. The Iron Age in northwestern Iran (9th to 3rd centuries BC) is characterized by the development of several significant urban centers around Lake Urmia related to the Manaeen kingdom and Median and Persian Empires (e.g., Daryaee 2011;

Fahimi 2019; Maziar 2019). The most important pollen evidence to the established sedentism and urban development is provided by the peaks of cultivated trees (Bottema and Woldring 1990; Djamali et al. 2021). This period is also correlated to successive peaks of wetland pollen types and higher precipitations (Figs. 4j and 6b). The main peak of arboriculture centered around 1700–1500 years BP corresponds well with the early and middle part of the Sasanian Empire (224–651 AD), while the decline of arboriculture that began around 1300 years BP corresponds to the Arab invasion of Iran and the fall of the Sasanian Empire (Djamali et al. 2021). Sasanian period is characterized by socio-economic prosperity of Persia and expansion of agriculture and urbanism all over the Iranian plateau (Djamali et al. 2016; Shumilovskikh et al. 2017).

Atmospheric teleconnection to the climate of the North Atlantic

Down-core abundances of Al (Fig. 6d) in the sediment core appear to co-vary with the Holocene record of ice rafted debris (IRD) events from North Atlantic sediments (Fig. 6e) (Bond et al. 1997) and intervals of reduced solar irradiance (Fig. 6f) (Bond et al. 2001; Solanki et al. 2004). Since these time series are based on different age models, have different resolutions, and represent various aspects of the climate system, the peak-to-peak correlation between them is not straightforward. However, wavelet analyses of these time series revealed similar periodicities (Fig. SI-2) suggesting noticeable co-variability between them.

This suggests the existence of an atmospheric teleconnection between North Atlantic climate and the interior of West Asia throughout the Holocene. A similar teleconnection on millennial timescales during the last glacial period has previously been observed between the North Atlantic, the interior of West Asia and the northern Indian Ocean (Schulz et al. 1998; Altabet et al. 2002; Pourmand et al. 2005, 2007; Sharifi et al. 2015). Further support for teleconnections between Urmia climate and that of the North Atlantic also comes from the time series study of modern climate data from NW Iran (Jalili et al. 2011; Zoljoodi and Didevarasl 2014; Alizadeh-Choobari et al. 2016; Sharifi et al. 2021).

We interpret the absence of any major evaporite horizons during the Holocene to represent the “natural” evolution of the sedimentary regime within the lake's catchment and depositional basins. It has been previously demonstrated that the lake's hydrological regime has been significantly altered by humans over the last half century (AghaKouchak et al. 2015; Sharifi et al. 2018b, 2021; Khazaei et al. 2019). The combination of modern and paleoclimate reconstruction now emphasizes the outsized role human activities have played in the demise of the lake in modern times.

Conclusions

A high-resolution multi-proxy reconstruction of climate and hydrologic conditions over Urmia Lake indicates several lake-level fluctuations since the Early Holocene. More frequent times of low lake levels during the Mid- and Late Holocene coincide with episodes of enhanced aeolian input and low riverine input to the lake. The expansion and contraction of wetland vegetation in the lake basin inferred from pollen data confirms the geochemical interpretation of lake hydrologic variations during the Holocene. In addition, there is general agreement between proxy interpretation from Urmia Lake with other regional records from high-altitude peat deposits from NW Iran and from the eastern Mediterranean Sea. Furthermore, the correlation between the Urmia Lake record and variations in North Atlantic climate and changes in solar irradiance suggest the sensitivity of Urmia Lake hydrology to internal and external forcing that controls the climate of the northern hemisphere, as well as an atmospheric teleconnection between the North Atlantic and the interior of West Asia during the last deglaciation. Although the general increasing trends in agro-pastoralism and urban development have continued since the Iron Age in the Urmia Lake region, there is a notable correlation between periods of more moisture availability and higher agricultural and urban development, strongly suggesting a hydroclimatic impact on civilizations in the Urmia Lake basin.

Although the moisture availability has changed since the beginning of the Holocene, our paleorainfall reconstruction for the Urmia Lake watershed has fluctuated within the range comparable to modern times. Taken together with the geochemical and pollen reconstructions, the absence of evaporative horizons from the entirety of this core that spans the Holocene strongly suggest that the contribution of natural climate cycles may have less influence on water availability to the lake today than the well documented impacts of extensive anthropogenic activities over the last few decades.

Supplementary Information The online version contains supplementary material available at <https://doi.org/10.1007/s10113-023-02119-x>.

Acknowledgements The authors thank Naser Ghasemi, Majid Pourkerman, and Mehdi Moradi for their extensive support during the fieldwork. Dahvya Belkacem is also thanked for assisting in laboratory pollen extraction.

Author contribution A. S. and A. P. designed the study. Fieldwork and sampling were conducted by A. S. and H. A. K. L. organized the expedition. X. R. F. analysis of cores and data interpretation performed A. S. and L. C. P. Pollen extraction and data interpretation were performed by M. D., M. G. P. A., and J. L. B. Geochemical analyses were performed by A. S., A. P., and P. K. S. DEM model and GIS mapping was conducted by M. E. A. S. wrote the original draft of the manuscript. All authors equally contributed to the article and approved the submitted version.

Funding This research was supported by the National Science Foundation grant EAR-1003639 to A. Pourmand and by a Geological Society of America Graduate Student Research Grant to A. Sharifi. The field campaign was supported by INIOAS project No 391-012-01.

Data availability The authors confirm that the data supporting the findings of this study are available within the article and its supplementary materials. These data are additionally available online: <https://zenodo.org/record/7240650#.Y1SvIuTMI5k>.

Declarations

Competing interests The authors declare no competing interests.

References

- AghaKouchak A, Norouzi H, Madani K, Mirchi A, Azarderakhsh M et al (2015) Aral Sea Syndrome Desiccates Lake Urmia: Call for Action. *J Great Lakes Research* 41:307–311. <https://doi.org/10.1016/j.jglr.2014.12.007>
- Algeo TJ, Maynard JB (2004) Trace-element behavior and redox facies in core shales of Upper Pennsylvanian Kansas-type cyclothems. *Chem Geol* 206:289–318. <https://doi.org/10.1016/j.chemgeo.2003.12.009>
- Alizadeh-Choobari O, Ahmadi-Givi F, Mirzaei N, Owlad E (2016) Climate change and anthropogenic impacts on the rapid shrinkage of Lake Urmia. *Int J Climatol* 36:4276–4286. <https://doi.org/10.1002/joc.4630>
- Altabet MA, Higginson MJ, Murray DW (2002) The effect of millennial-scale changes in Arabian Sea denitrification on atmospheric CO₂. *Nature* 415:159–162. <https://doi.org/10.1038/415159a>
- Beug HJ (2004) Leitfaden der Pollenbestimmung für Mitteleuropa und angrenzende Gebiete. Verlag Dr Friedrich Pfeil, München
- Bond G, Showers W, Cheseby M, Lotti R, Almasi P et al (1997) A pervasive millennial-scale cycle in north Atlantic holocene and glacial climates. *Science* (80-) 278(5341):1257–1266. <https://doi.org/10.1126/science.278.5341.1257>
- Bond G, Kromer B, Beer J, Muscheler R, Evans MN et al (2001) Persistent solar influence on North Atlantic climate during the Holocene. *Science* 294:2130–2136. <https://doi.org/10.1126/science.1065680>
- Bottema S (1986) A late quaternary pollen diagram from Lake Urmia (Northwestern Iran). *Rev Palaeobot Palynol* 47:241–261. [https://doi.org/10.1016/0034-6667\(86\)90039-4](https://doi.org/10.1016/0034-6667(86)90039-4)
- Bottema S, Woldring W (1990) Anthropogenic indicators in the pollen diagrams of the Eastern Mediterranean. In: Bottema S, Entjes-Nieborg G, van Zeist W (eds) Man's role in the shaping of the Eastern Mediterranean landscape. Balkema, Rotterdam, pp 231–264
- Brown ET (2011) Lake Malawi's response to "megadrought" terminations: sedimentary records of flooding, weathering and erosion. *Palaeogeogr Palaeoclimatol Palaeoecol* 303:120–125. <https://doi.org/10.1016/j.palaeo.2010.01.038>
- Calvert SE, Pedersen TF (2007) Elemental proxies for palaeoclimatic and palaeoceanographic variability in marine sediments: interpretation and application. In: Hillaire-Marcel C, Vernal AD (eds) Proxies in Late Cenozoic Paleoclimatology. Elsevier, Amsterdam, pp 567–644
- Calvert SE, Pedersen TF (1993) Geochemistry of recent oxic and anoxic marine sediments: Implications for the geological record. *Mar Geol* 113:67–88. [https://doi.org/10.1016/0025-3227\(93\)90150-T](https://doi.org/10.1016/0025-3227(93)90150-T)

- Daryae T (2011) *The Oxford handbook of Iranian history*, 1st edn. Oxford University Press Inc., New York
- Degens ET, Wong HK, Kempe S, Kurtman F (1984) A geological study of lake van, Eastern Turkey. *Geol Rundschau* 73:701–734. <https://doi.org/10.1007/BF01824978>
- Djamali M, de Beaulieu J-L, Shah-hosseini M, Andrieu-Ponel V, Ponel P et al (2008) A late Pleistocene long pollen record from Lake Urmia, NW Iran. *Quat Res* 69(3):413–420. <https://doi.org/10.1016/j.yqres.2008.03.004>
- Djamali M, Kürschner H, Akhiani H, de Beaulieu JL, Amini A et al (2008b) Palaeoecological significance of the spores of the liverwort *Riella* (Riellaceae) in a late Pleistocene long pollen record from the hypersaline Lake Urmia, NW Iran. *Rev Palaeobot Palynol* 152(1–2):66–73. <https://doi.org/10.1016/j.revpalbo.2008.04.004>
- Djamali M, Akhiani H, Andrieu-Ponel V, Braconnot P, Brewer S et al (2010) Indian summer monsoon variations could have affected the early-holocene woodland expansion in the Near East. *The Holocene* 20(5):813–820. <https://doi.org/10.1177/0959683610362813>
- Djamali M, Ponel P, Delille T, Thiery A, Asem A et al (2010b) A 200,000-year record of the brine shrimp *Artemia* (Crustacea: Anostraca) remains in Lake Urmia, NW Iran. *Int J Aquat Sci* 1:14–18
- Djamali M, Jones MD, Migliore J, Balatti S, Fader M et al (2016) Olive cultivation in the heart of the Persian Achaemenid Empire: new insights into agricultural practices and environmental changes reflected in a late Holocene pollen record from Lake Parishan, SW Iran. *Veg Hist Archaeobot* 25(3):255–269. <https://doi.org/10.1007/s00334-015-0545-8>
- Djamali M, Saeidi Ghavi Andam S, Poschlod P (2021) An update on the history of arboriculture in Ancient Iran. In: Balatti S, Klinkottand H, Wiesehöfer J (eds) *Paleopersepolis environment, landscape and society in ancient Fars*. Franz Steiner Verlag, Stuttgart, pp 121–132
- Eimanifar A, Mohebbi F (2007) Urmia Lake (Northwest Iran): a brief review. *Saline Syst* 3:5. <https://doi.org/10.1186/1746-1448-3-5>
- Fahimi H (2019) The Bronze Age and the Iron Age on the Central Iranian Plateau. Two successive cultures or the appearance of a new culture? In: Meyer J-W, Vila E, Mashkour M, et al. (eds) *The Iranian Plateau during the Bronze Age. Development of Urbanisation, Production and Trade. MAISON DE L'ORIENT ET DE LA MÉDITERRANÉE – JEAN-POUILLOUX*, pp 201–216
- Farsnews (2011) Ahmadinejad: “current condition at Urmia Lake appears every 500 years”. In: Fars News Agency. <https://www.farsnews.com/news/13900625000278>. Accessed 5 Sep 2016
- Fritz S (1996) Paleolimnological records of climatic change in North America. *Limnol Oceanogr* 41:882–889. <https://doi.org/10.4319/lo.1996.41.5.0882>
- Govin A, Holzwarth U, Heslop D, Ford Keeling L, Zabel M et al (2012) Distribution of major elements in Atlantic surface sediments (36°N–49°S): Imprint of terrigenous input and continental weathering. *Geochemistry, Geophys Geosystems* 13(1):1–23. <https://doi.org/10.1029/2011GC003785>
- Grimm EC (1992) *Tilia 2.0 and Tilia × graph 1.18*. Illinois State Museum, Research and Collection Center, Springfield
- Guibal F, Lak R, de Beaulieu J-L, Andrieu-Ponel V, Berberian M et al (2014) Notes on arboricultural and agricultural practices in ancient Iran based on new pollen evidence. *Paléorient* 36(2):175–188. <https://doi.org/10.3406/paleo.2010.5394>
- Harmon RS, Wörner G, Goldsmith ST, Harmon BA, Gardner CB et al (2016) Linking silicate weathering to riverine geochemistry — A case study from a mountainous tropical setting in west-central Panama. *Geol Soc Am Bull* 128(11–12):1780–1812. <https://doi.org/10.1130/B31388.1>
- Harrison SP, Kohfeld KE, Roelandt C, Claquin T (2001) The role of dust in climate changes today, at the last glacial maximum and in the future. *Earth Sci Rev* 54:43–80. [https://doi.org/10.1016/S0012-8252\(01\)00041-1](https://doi.org/10.1016/S0012-8252(01)00041-1)
- Haslett J, Parnell A (2008) A simple monotone process with application to radiocarbon-dated depth chronologies. *J R Stat Soc Ser C Applied Stat* 57:399–418. <https://doi.org/10.1111/j.1467-9876.2008.00623.x>
- Hassanzadeh E, Zarghami M, Hassanzadeh Y (2012) Determining the main factors in declining the Urmia Lake level by using system dynamics modeling. *Water Resour Manag* 26:129–145. <https://doi.org/10.1007/s11269-011-9909-8>
- Jalili S, Morid S, Banakar A, Namdar Qanbari R (2011) Assessing the effect of SOI and NAO indices on Lake Urmia water level variations, application of spectral analysis. *J Water Soil* 25:140–149 (in Persian with English abstract)
- Jiménez-Espejo FJ, García-Alix A, Jiménez-Moreno G, Rodrigo-Gámiz M, Anderson RS et al (2014) Saharan aeolian input and effective humidity variations over western Europe during the Holocene from a high altitude record. *Chem Geol* 374–375:1–12. <https://doi.org/10.1016/j.chemgeo.2014.03.001>
- Kaniewski D, Paulissen E, Van Campo E, Weiss H, Otto T et al (2010) Late second–early first millennium BC abrupt climate changes in coastal Syria and their possible significance for the history of the Eastern Mediterranean. *Quat Res* 74(2):207–215. <https://doi.org/10.1016/j.yqres.2010.07.010>
- Kaniewski D, Marriner N, Cheddadi R, Morhange C, Bretschneider J et al (2019) Cold and dry outbreaks in the eastern Mediterranean 3200 years ago. *Geology* 47(10):933–937. <https://doi.org/10.1130/G46491.1>
- Kelts K, Shahrabi M (1986) Holocene sedimentology of, Hypersaline Lake Urmia, Northwestern Iran. *Palaeogeogr Palaeoclimatol Palaeoecol* 54:105–130. [https://doi.org/10.1016/0031-0182\(86\)90120-3](https://doi.org/10.1016/0031-0182(86)90120-3)
- Khabaronline News Agency (2011) President Ahmadinejad: “Urmia Lake has experienced the same condition 500 years ago”. In: Khabaronline News Agency. khabaronline.ir/news/173553. Accessed 16 Jan 2019
- Khazaei B, Khatami S, Alemohammad SH, Rashidi L, Wu C et al (2019) Climatic or regionally induced by humans? Tracing hydro-climatic and land-use changes to better understand the Lake Urmia tragedy. *J Hydrol* 569:203–217. <https://doi.org/10.1016/j.jhydrol.2018.12.004>
- Kuzucuoğlu C, Dorfler W, Kunesch S, Goupille F (2011) Mid- to Late-Holocene climate change in central Turkey: the Tecer Lake record. *Holocene* 21:173–188. <https://doi.org/10.1177/0959683610384163>
- Lourens LJ, Wehausen R, Brumsack HJ (2001) Geological constraints on tidal dissipation and dynamical ellipticity of the Earth over the past three million years. *Lett to Nat* 409:1029–1033
- Manaffar R, Zare S, Agh N, Siyabgodsí A, Soltanian S et al (2011) Sediment cores from Lake Urmia (Iran) suggest the inhabitation by parthenogenetic *Artemia* around 5,000 years ago. *Hydrobiologia* 671:65–74. <https://doi.org/10.1007/s10750-011-0704-6>
- Martínez-Ruiz F, Kastner M, Gallego-Torres D, Rodrigo-Gámiz M, Nieto-Moreno V, et al (2015) Paleoclimate and paleoceanography over the past 20,000yr in the Mediterranean Sea Basins as indicated by sediment elemental proxies. *Quat Sci Rev* 107:25–46. <https://doi.org/10.1016/j.quascirev.2014.09.018>
- Mayewski PA, Rohling EE, Stager JC, Maasch KA, Meeker LD et al (2004) Holocene climate variability. *Quat Res* 62:243–255. <https://doi.org/10.1016/j.yqres.2004.07.001>
- Maziar S (2019) Iran and the Kura-Araxes cultural tradition, so near and yet so far. In: Meyer J-W, Vila E, Mashkour M, Casanova M, Vallet R (eds) *The Iranian Plateau during the Bronze Age*.

- Development of Urbanisation, Production and Trade. MAISON DE L'ORIENT ET DE LA MÉDITERRANÉE – JEAN POUILLoux, pp 51–74
- McKenzie D (1972) Active tectonics of the Mediterranean region. *GeophysJRAstronSoc* 30:109–185. <https://doi.org/10.1111/j.1365-246x.1972.tb02351.x>
- McKenzie D (1976) The East Anatolian Fault: a major structure in Eastern Turkey. *Earth Planet Sci Lett* 29:189–193. <https://doi.org/10.1136/bmj.2.3908.1076>
- Mehterian S, Pourmand A, Sharifi A, Lahijani HAK, Naderi M et al (2017) Speleothem records of glacial/interglacial climate from Iran forewarn of future Water Availability in the interior of the Middle East. *Quat Sci Rev* 164:187–198. <https://doi.org/10.1016/j.quascirev.2017.03.028>
- Meunier A, Caner L, Hubert F, El Albani A, Pret D (2013) The weathering intensity scale (WIS): An alternative approach of the chemical index of alteration (CIA). *Am J Sci* 313(2):113–143. <https://doi.org/10.2475/02.2013.03>
- Middleton NJ (1986) A geography of dust storms in South-West Asia. *Int J Climatol* 6:183–196. <https://doi.org/10.1002/joc.3370060207>
- Migowski C, Stein M, Prasad S, Negendank JFW, Agnon A (2006) Holocene climate variability and cultural evolution in the Near East from the Dead Sea sedimentary record. *Quat Res* 66(3):421–431. <https://doi.org/10.1016/j.yqres.2006.06.010>
- Miot J, Jézéquel D, Benzerara K, Cordier L, Rivas-Lamelo S, Skouripantet F et al (2016) Mineralogical Diversity in Lake Pavin: Connections with Water Column Chemistry and Biomineralization Processes. *Minerals* 6(2):24. <https://doi.org/10.3390/min6020024>
- Moore PD, Webb JA, Collinson ME (1991) Pollen analysis. Blackwell Scientific Publications, Oxford, Second Edi
- Muhs DR, Bettis EA, Been J, McGeehin JP (2001) Impact of climate and parent material on chemical weathering in Loess-derived soils of the Mississippi River Valley. *Soil Sci Soc Am J* 65:1761. <https://doi.org/10.2136/sssaj2001.1761>
- Myers TS, Tabor NJ, Rosenau NA (2014) Multiproxy approach reveals evidence of highly variable paleoprecipitation in the Upper Jurassic Morrison Formation (western United States). *Bull Geol Soc Am* 126:1105–1116. <https://doi.org/10.1130/B30941.1>
- Nesbitt HW, Young GM (1982) Early Proterozoic climate and plate motions inferred from major element chemistry of lutites. *Nature* 299:715–717
- Nesbitt HW, Young GM (1989) Formation and diagenesis of weathering profiles. *J Geol* 97:129–146
- Nieto-Moreno V, Martínez-Ruiz F, Giralt S, Jiménez-Espejo F, Gallego-Torres D et al (2011) Tracking climate variability in the western Mediterranean during the Late Holocene: a multiproxy approach. *Clim Past* 7(4):1395–1414. <https://doi.org/10.5194/cp-7-1395-2011>
- Nordt LC, Driese SD (2010) New weathering index improves paleorainfall estimates from Vertisols. *Geology* 38:407–410. <https://doi.org/10.1130/G30689.1>
- Parnell AC, Haslett J, Allen JRM, Buck CE, Huntley B (2008) A flexible approach to assessing synchronicity of past events using Bayesian reconstructions of sedimentation history. *Quat Sci Rev* 27:1872–1885. <https://doi.org/10.1016/j.quascirev.2008.07.009>
- Pourmand A, Marcantonio F, Bianchi TS, Canuel E a., Waterson EJ (2005) Radionuclide and biomarker proxies of past ocean circulation and productivity in the Arabian Sea. *Geophys Res Lett* 32(10):1–4. <https://doi.org/10.1029/2005GL022612>
- Pourmand A, Marcantonio F, Bianchi TS, Canuel E a., Waterson EJ (2007) A 28-ka history of sea surface temperature, primary productivity and planktonic community variability in the western Arabian Sea. *Paleoceanography* 22(4):PA4208 1–14. <https://doi.org/10.1029/2007PA001502>
- Prospero JM, Ginoux P, Torres O, Nicholson SE, Gill TE (2002) Environmental characterization of global sources of atmospheric soil dust identified with the NIMBUS 7 Total Ozone Mapping Spectrometer (TOMS) absorbing aerosol product. *Rev Geophys* 40:1–31. <https://doi.org/10.1029/2000RG000095>
- Reille M (1992) Pollen et spores d'Europe et d'Afrique du Nord. Laboratoire de botanique historique et de palynologie. Laboratoire de Botanique historique et Palynologie, Marseille
- Reille M (1995) Pollen et spores d'Europe et d'Afrique du Nord. Laboratoire de botanique historique et de palynologie-Supplément 1. Laboratoire de Botanique historique et Palynologie, Marseille
- Reille M (1998) Pollen et spores d'Europe et d'Afrique du Nord. Laboratoire de botanique historique et de palynologie-Supplément 2. Laboratoire de Botanique historique et Palynologie, Marseille
- Reimer PJ, Austin WEN, Bard E, Bayliss A, Blackwell PG, et al (2020) The IntCal20 Northern hemisphere radiocarbon age calibration curve (0-55 cal kBP). *Radiocarbon* 62(4):725–757. <https://doi.org/10.1017/RDC.2020.41>
- Rezvantalab S, Amrollahi MH (2011) Investigation of recent changes in Urmia Salt Lake. *Int J Chem Environ Eng* 2:168–171
- Rivas-Martínez S, Sánchez-Mata D, Costa M (1999) North American boreal and western temperate forest vegetation (syntaxonomical synopsis of the potential natural plant communities of North America II). *Itinera Geobot* 12:5–316
- Rodrigo-Gámiz M, Martínez-Ruiz F, Rodríguez-Tovar FJ, Jiménez-Espejo FJ, Pardo-Igúzquiza E (2014) Millennialto centennial-scale climate periodicities and forcing mechanisms in the westernmost Mediterranean for the past 20,000 yr. *Quat Res (United States)* 81(1):78–93. <https://doi.org/10.1016/j.yqres.2013.10.009>
- Schilman B, Bar-Matthews M, Almogi-labin A, Luz B (2001) Global climate instability reflected by Eastern Mediterranean marine records during the late Holocene. *Palaeogeogr Palaeoclimatol Palaeoecol* 176:157–176. [https://doi.org/10.1016/S0031-0182\(01\)00336-4](https://doi.org/10.1016/S0031-0182(01)00336-4)
- Schulz H, von Rad U, Erlenkeuser H (1998) Correlation between Arabian Sea and Greenland climate oscillations of the past 110,000 years: Nature. *Nature* 393:54–62. <https://doi.org/10.1038/31750>
- Shah-Hosseini M (2003) Sedimentology of hypersaline Lake Urmia in central part of Shahid Kalantari highway with special reference to their origin. M Sc Thesis, Geology Department University of Tehran, p 88
- Shahrabi M (1994) Seas and Lakes of Iran. Geological Survey of Iran, Treatise on Geology of Iran, Book No. 10, Tehran
- Sharifi A, Pourmand A, Canuel EA, Ferer-Tyler E, Peterson LC et al (2015) Abrupt climate variability since the last deglaciation based on a high-resolution, multi-proxy peat record from NW Iran: The hand that rocked the Cradle of Civilization? *Quat Sci Rev* 123:215–230. <https://doi.org/10.1016/j.quascirev.2015.07.006>
- Sharifi A, Murphy LN, Pourmand A, Clement AC, Canuel EA et al (2018) Early-Holocene greening of the Afro-Asian dust belt changed sources of mineral dust in West Asia. *Earth Planet Sci Lett* 481:30–40. <https://doi.org/10.1016/j.epsl.2017.10.001>
- Sharifi A, Shah-hosseini M, Pourmand A, Esfahaninejad M (2018) The vanishing of urmia Lake: A geomnological perspective on the hydrological imbalance of the World 's second largest hypersaline lake. In: Nooran PG et al (eds) Lake Urmia: A Hypersaline waterbody in a drying climate. Springer Nature Switzerland, pp 1–38. https://doi.org/10.1007/978_94_007_698_359
- Sharifi A, Esfahaninejad M, Kabiri K (2021) Hydroclimate of the Lake Urmia catchment area: A brief overview. In: Peygham G, Nooran, Evgeniy V, Yakushev OAN and JB (eds) Lake Urmia:

- A hypersaline waterbody in a drying climate. Springer Nature Switzerland. https://doi.org/10.1007/698_2021_809
- Sheldon ND, Retallack GJ, Tanaka S (2002) Geochemical climofunctions from North American soils and application to Paleosols across the Eocene-Oligocene boundary in Oregon. *J Geol* 110:687–696. <https://doi.org/10.1086/342865>
- Shumilovskikh L, Djamali M, Andrieu-Ponel V, Ponel P, Beaulieu J et al (2017) Palaeoecological insights into agri-horti-cultural and pastoral practices before, during and after the Sasanian Empire. In: Sauer E (ed) *Sasanian Persia: Between Rome and the Steppes of Eurasia*. University Press, Edinburgh, pp 51–73
- Sima S, Ahmadalipour A, Tajrishy M (2013) Mapping surface temperature in a hyper-saline lake and investigating the effect of temperature distribution on the lake evaporation. *Remote Sens Environ* 136:374–385. <https://doi.org/10.1016/j.rse.2013.05.014>
- Solanki SK, Usoskin IG, Kromer B, Schüssler M, Beer J (2004) Unusual activity of the Sun during recent decades compared to the previous 11,000 years. *Nature* 431(7012):1084–1087. <https://doi.org/10.1038/nature02995>
- Stallard RF (1985) River chemistry, geology, geomorphology and soils in the Amazon and Orinoco Basins. In: Drever JI (ed) *The Chemistry of Weathering*. N.A.T.O. Advanced Science Institutes Series. D. Reidel, Dordrecht, pp 324–345
- Stevens LR, Djamali M, Andrieu-Ponel V, Beaulieu J-L (2012) Hydroclimatic variations over the last two glacial/interglacial cycles at Lake Urmia, Iran. *J Paleolimnol* 47:645–660. <https://doi.org/10.1007/s10933-012-9588-3>
- Stockmarr J (1971) Tablets with spores used in absolute pollen analysis. *Pollen et Spores* 13:615–621
- Street-Perrott FA, Roberts N (1983) Fluctuations in closed basin lakes as an indicator of past atmospheric circulation patterns. In: Street-Perrott A, Beran M, Robert R (eds) *Variations in the Global Water Budget*. Springer, Netherlands, pp 331–345
- Stuiver M, Reimer PJ, Reimer RW (2021) CALIB rev. 8.2; Stuiver, M, and Reimer PJ, 1993. *Radiocarbon* 35:215–230
- Talebi T, Ramezani E, Djamali M, Lahijani HAK, Naqinezhad A et al (2016) The Late-Holocene climate change, vegetation dynamics, lake-level changes and anthropogenic impacts in the Lake Urmia region, NW Iran. *Quat Int* 408:40–51. <https://doi.org/10.1016/j.quaint.2015.11.070>
- Team Rs (2015) RStudio: integrated development for R. <https://www.rstudio.com/>
- Torrence C, Compo GP (1995) A practical guide to wavelet analysis. *Bull Am Meteorol Soc* 79(1):61–78. [https://doi.org/10.1175/1520-0477\(1998\)079%3c0061:APGTWA%3e2.0.CO;2](https://doi.org/10.1175/1520-0477(1998)079%3c0061:APGTWA%3e2.0.CO;2)
- Tudryn A, Motavalli-anbaran S, Tucholka P, Gibert-brunet E (2021) Late Quaternary environmental changes of Lake Urmia basin (NW Iran) inferred from sedimentological and magnetic records. *Quat Int*. <https://doi.org/10.1016/j.quaint.2021.03.024>
- Van Zeist W, Bottema S (1977) Palynological investigations in western Iran. *Palaeohistoria*, pp 19–85
- Wick L, Lemcke G, Sturm M (2003) Evidence of Lateglacial and Holocene climatic change and human impact in eastern Anatolia: high-resolution pollen, charcoal, isotopic and geochemical records from the laminated sediments of Lake Van, Turkey. *Holocene* 13:665–675. <https://doi.org/10.1191/0959683603hl653rp>
- Zoljoodi M, Didevarasl A (2014) Water-level fluctuations of Urmia Lake: relationship with the long-term changes of meteorological variables (solutions for water-crisis management in Urmia Lake Basin). *Atmos Clim Sci* 04:358–368. <https://doi.org/10.4236/acs.2014.43036>

Supplementary Information for

The Rise and Demise of Iran's Urmia Lake during the Holocene and the Anthropocene: "What's past is prologue"

Arash Sharifi, Morteza Djamali, Larry C. Peterson, Peter K. Swart, María Guadalupe Pulido Ávila, Mojgan Esfahaninejad, Jacques-Louis de Beaulieu, Hamid A. K. Lahijani, Ali Pourmand

Corresponding authors: Arash Sharifi osharifi@earth.miami.edu,

Ali Pourmand apourmand@earth.miami.edu

This PDF file includes:

Fig. S-1

Fig. S-2

Core Logs

Other supplementary materials for this manuscript include the following:

Datasets S-1

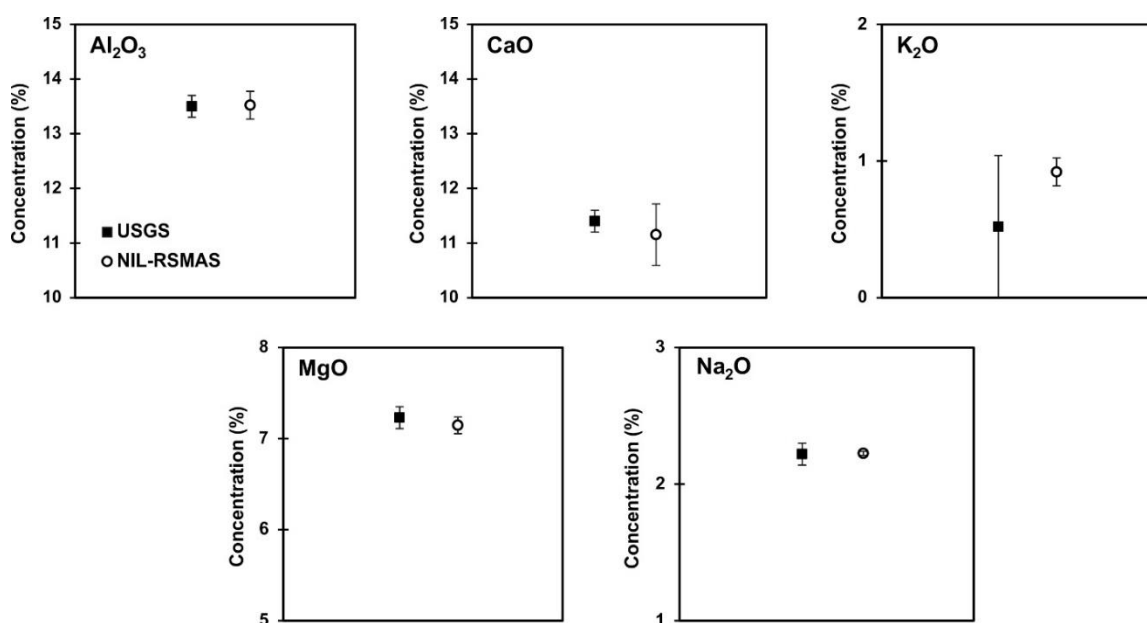


Fig. S-1- Replicate measurements of major oxide concentrations (%) for USGS CRM BHVO-2 at the Neptune Isotope Lab (NIL-RSMAS, open circle) are comparable within uncertainties to the mean values from literature compilation (USGS, Solid Square), data from GEOREM, <http://georem.mpch-mainz.gwdg.de/>. Uncertainties are reported as the relative standard deviation.

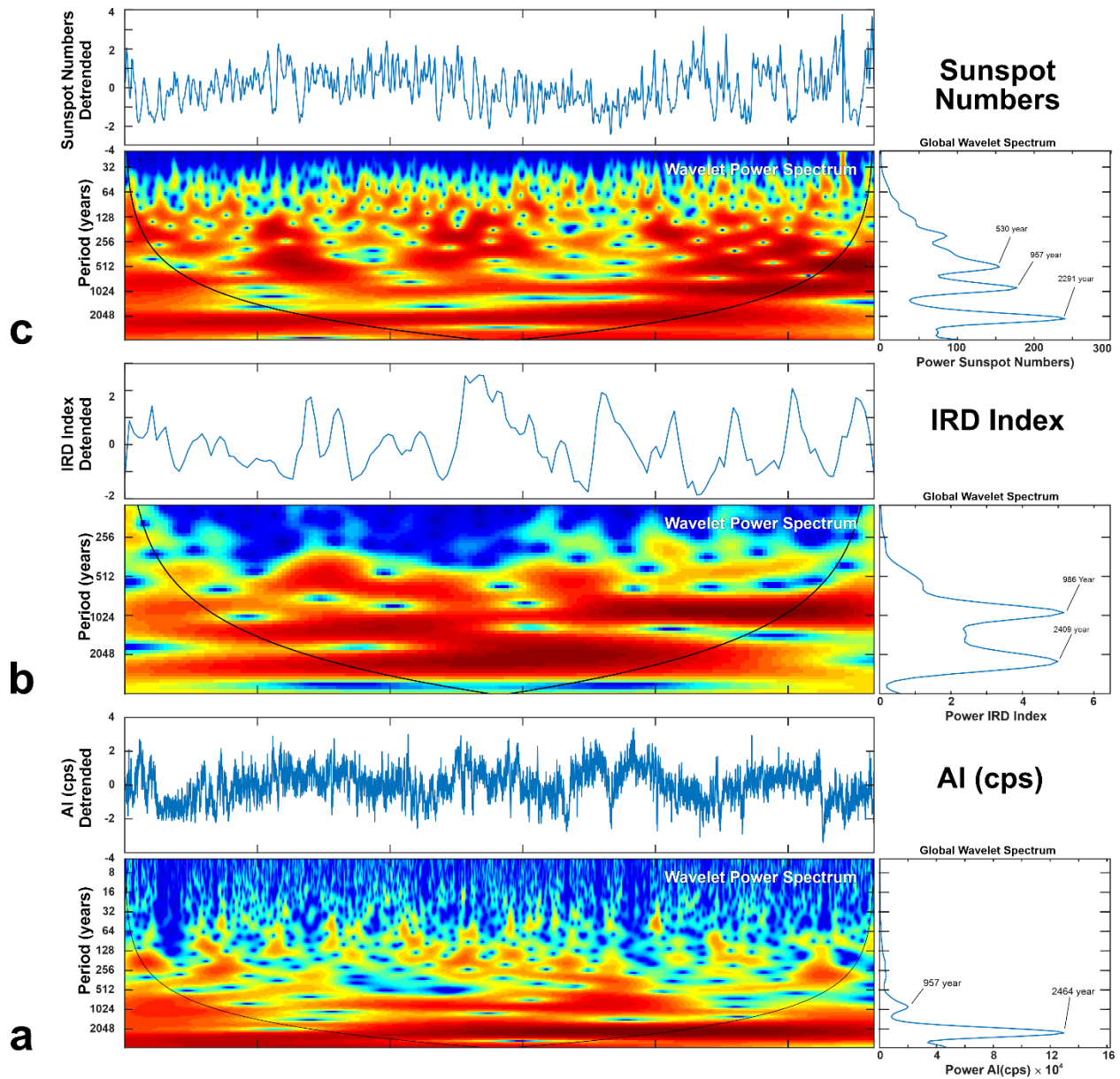


Fig. S-2- Wavelet power spectrum of detrended Al-XRF variations (a) in count per second (cps), North Atlantic Holocene Ice Rafted Debris (IRD) Index (b) (Bond et al., 2001, 1997) (b), and 11 ka reconstruction of sunspot numbers (c) (Solanki et al., 2004). Solid lines in wavelet power spectrum panels denote the cone of influence. The global power spectrum with the most significant peak of spectral power is shown on the right panel

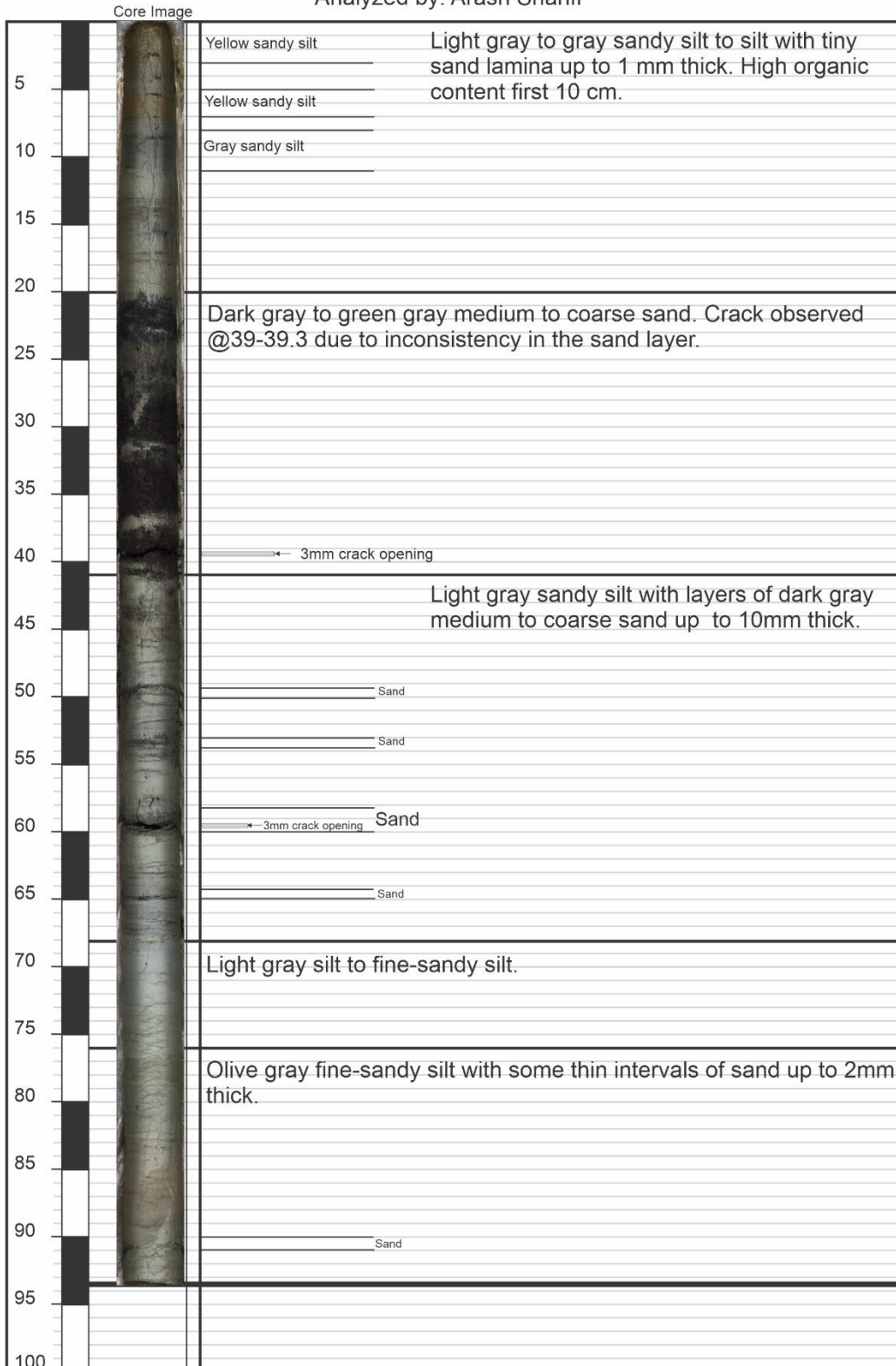
Core Logs: Detailed visual description of different segments (1 to 5) of the 5-m long core used in this study.

Core No.:U6-1

Location: Urmia Lake-IRAN End of the Core @ 93.5 cm

Date:11-17-2012

Analyzed by: Arash Sharifi

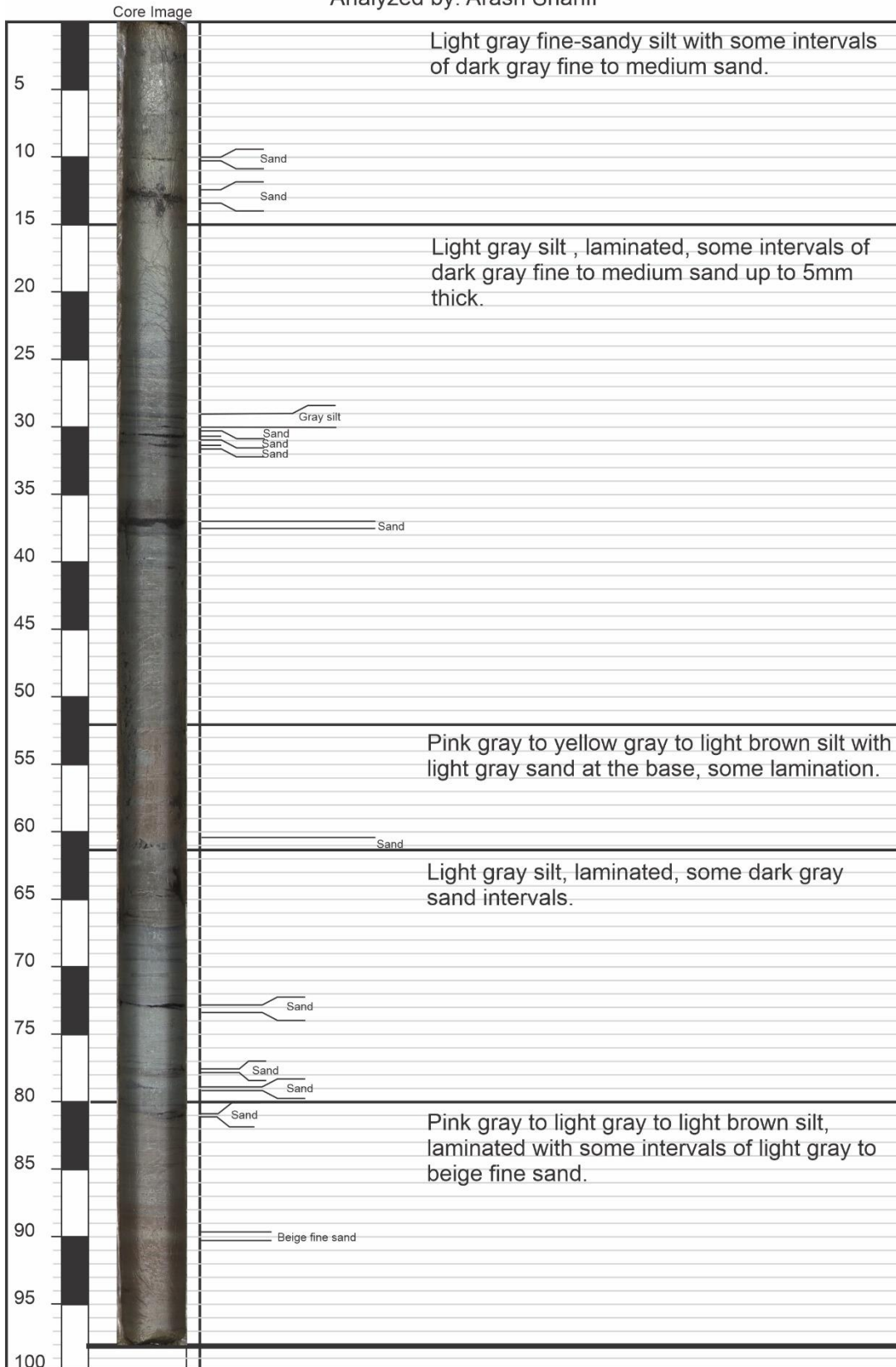


Core No.:U6-3

Location: Urmia Lake-IRAN End of the Core @ 98 cm

Date:11-18-2012

Analyzed by: Arash Sharifi



Core No.:U6-5

Location: Urmia Lake-IRAN End of the Core @ 99 cm

Date:11-17-2012

Analyzed by: Arash Sharifi

